

Article

Tribological Analysis of Several Coatings under Flood and Cryogenic Cooling Conditions

Yutao Zhang ¹, Jose C. Outeiro ^{1,2,*}, Corinne Nouveau ¹, Bertrand Marcon ¹ and Lamice A. Denguir ³

¹ LABOMAP, Arts et Metiers Institute of Technology, Université Bourgogne Franche-Comté, HESAM Université, F-71250 Cluny, France; yutao.zhang@ensam.eu (Y.Z.); corinne.nouveau@ensam.eu (C.N.); bertrand.marcon@ensam.eu (B.M.)

² Department of Mechanical Engineering and Engineering Science, University of North Carolina at Charlotte, Charlotte, NC 28223, USA

³ Knowledge and Skills, F-71000 Macon, France; lamice.denguir@gmail.com

* Correspondence: jc.outeiro@charlotte.edu

Abstract: The contact between the tool and the workpiece/chip in metal cutting is complex, resulting in high local temperatures and stresses, which may cause severe tool wear and failure. Developments in cryogenic-assisted machining have shown an ecological alternative to the classical metal working fluids, besides tool wear reduction during machining difficult-to-cut materials due to the good ability to dissipate the heat generated by this process. The objective of this work is to analyze the tribological conditions and performance of new coatings specially developed for cryogenic-assisted machining in terms of friction coefficient, volume of build-up material (adhesion) to the tool, and tool temperature. The results have shown that the sliding speed and cooling/lubrication strategy are two main factors that affect the friction coefficient and adhesion of Ti-6Al-4V alloy to the pins. These tribological tests should allow us to select the best coating(s) to be used in cutting tools for further tool wear analysis. Moreover, the obtained friction coefficients could be further implemented into metal cutting models to predict the machining outcomes, including the surface integrity of the machined parts and tool wear.

Keywords: tribology; friction; machining; cryogenic assisted machining; coatings; Ti-6Al-4V



Citation: Zhang, Y.; Outeiro, J.C.; Nouveau, C.; Marcon, B.; Denguir, L.A. Tribological Analysis of Several Coatings under Flood and Cryogenic Cooling Conditions. *Appl. Sci.* **2023**, *13*, 11743. <https://doi.org/10.3390/app132111743>

Academic Editor: Jacek Tomków

Received: 31 July 2023

Revised: 11 October 2023

Accepted: 16 October 2023

Published: 26 October 2023



Copyright: © 2023 by the authors. Licensee MDPI, Basel, Switzerland. This article is an open access article distributed under the terms and conditions of the Creative Commons Attribution (CC BY) license (<https://creativecommons.org/licenses/by/4.0/>).

1. Introduction

The contact between the tool and the chip/workpiece has a significant impact on tool life and the surface integrity. This contact strongly depends on several factors (contact conditions), including sliding speed, contact pressure, temperature, lubrication/cooling strategy, etc. [1,2]. The friction coefficient is often used to model this contact to correlate the shear stress with the normal stress acting at the tool–chip and tool–workpiece interfaces. This coefficient should be determined experimentally through specially designed tribological tests able to reproduce the contact conditions observed in metal cutting [3]. This is essential for the accurate simulation of the metal cutting process. Especially for the simulations when coated tools and cooling conditions are applied, the knowledge about the tribological behavior at the workpiece/chip interface is limited.

Unfortunately, classical methods for determining the friction coefficient between two instances based on pin-on-disc are not suitable to describe the tribological conditions in the metal cutting process. The standard pin-on-disc tribometer uses a pin to rub repeatedly over a rotating disc to determine the friction coefficient and the wear volume. However, the pins rub over the same surface of the disc at lower speed and contact pressure when compared to metal cutting process [4–6]. Two main approaches to investigate the tribological phenomena (including the determination of the friction coefficient) at the tool–chip interface can be found in the literature. One is using the cutting process itself [7–10]; apparently it is the best way to provide the relevant friction conditions, but this approach is not able to extract

quantitative results, because it is impossible to have first-hand information about the local contact pressure, sliding velocity or temperature. Even the approach based on analytical models linking the local shear strength, temperature or sliding velocity is not suitable, due to the limitations of these models, and to the large uncertainty in determining their parameters [11]. The second is based on specially designed tribometers able to reproduce the contact conditions in metal cutting [5,12,13]. A pin rubs on the refreshed surface of a workpiece in rotation, and the helical movement of the pin on the bar avoids the superposing of the scratch on the cylinder. So, the surface of the workpiece in contact with the pin is always different and never repeated where the contact area of the pin remains the same (as the cutting tool). Meanwhile, the workpiece needs to be refreshed each time. As mentioned by Rech et al. [3], such tribometers are able to reproduce the contact pressure, temperature and velocity between the tool and the chip in metal cutting, thus contributing to a better understanding of the tribological phenomena in this process.

The apparent friction coefficient is strongly correlated to the sliding speed and the contact pressure. Many researchers have shown that the friction coefficient drops when increasing the sliding speed [14–18]. Rech et al. [3] conducted tribological tests on various work materials with a TiN-coated carbide tool; the friction coefficient dropped significantly with increasing sliding speeds. Similar results were obtained by other researchers for other materials and contact conditions [4,11,19,20]. Besides this, the contact pressure between the pin and workpiece is also a crucial parameter that affects the friction coefficient. Meier et al. [21] tested the friction coefficient using different normal forces between 5 N and 400 N, under dry and flood conditions. Using lower loads, the friction coefficient increases with the sliding velocity. However, using higher loads, the friction coefficient decreases when the sliding speed increases.

Studies conducted on several metallic and non-metallic work materials using different gases and liquids as cooling/lubricant strategies have shown that the friction coefficient is the lowest when liquid nitrogen (LN_2) is used, followed by gaseous nitrogen and finally air [22–24]. But there are also contradictory studies showing that the low temperature induced by LN_2 will increase friction coefficient and wear rate [25,26]. It is also revealed that for some metallic materials, like aluminium, brass–lead pairs and self-mating niobium, the reduction in the friction coefficient and wear rate is significant [26]. Gradt et al. [23] found that the friction coefficient and wear rate decreased significantly in 8 K and 77 K He gas compared to in air at an ambient temperature (300 K) for polymer materials. In contrary, the modeling of the tribological behavior of titanium alloys [27] under cryogenic conditions using high loads and speeds shows that the friction coefficient of Ti6Al4V is higher than in air, as well as in the CFRP drilling procedure [28]. LN_2 and CO_2 are the two most frequently used very-low-temperature cooling methods in machining operations. Jerold and Kumar [29] reported that both LN_2 and CO_2 resulted in lower cutting temperatures compared to conventional flood MWF, but LN_2 (reduction of 47%) is more effective in reducing the temperature than CO_2 (reduction of 36%). Pahlitzsch [30] reported that LN_2 and CO_2 resulted in 240% and 150% longer tool lives compared to dry machining, respectively. Klocke et al. [31] reported that in turning Ti–6Al–4V titanium alloys, the use of LN_2 and CO_2 significantly improves the tool life compared to conventional flood MWF; in particular, the LN_2 increases the tool life five-fold. LN_2 can extend the tool life in the machining of titanium alloys at higher cutting speeds [32–38]. A comparison of the main advantages is shown in Table 1.

Table 1. Comparison of effectiveness and applications of various cooling and lubricant methods [39].

Effects of Cooling and Lubrication Method		CO ₂	LN ₂
Primary	Cooling	Good	Excellent
	Lubrication	Marginal	Marginal
	Chip removal	Good	Good
	Tool life	Good	Excellent
Secondary	Machine cooling	Marginal	Marginal
	Workpiece cooling	Good	Good
	Spray control	Marginal	Marginal
	Surface integrity	Good	Excellent

Gupta [40] reviewed various more environment-friendly cutting fluids, including cryogenic cooling, MQL, solid lubricants, etc. Pereira et al. [41] employed a combination of MQL + CO₂ in milling Inconel 718. Although conventional cutting fluids (mixtures oil–water) exhibited the best performance, from the ecological perspective MQL + CO₂ significantly reduces the amount of mineral oil by 90% in comparison with conventional cutting fluids.

The objective of this work is to investigate the tribological behaviors of several new multilayer coatings specially developed for the cryogenic-assisted machining of Ti–6Al–4V alloy. The coatings are CrN and AlCrN monolayers, as well as CrN/AlCrN-based multilayers with two different architectures. The choice of Cr-based coatings instead of the most common Ti-based coatings is justified by the higher corrosion resistance and, more importantly, good thermal properties of Cr-based ones. Rech et al. [42] investigated the tribological and thermal functions of various cutting tools coated by TiAlN, TiN and TiAlN + MoS₂. The results show that these coatings do not have a significant influence on heat transmission on the substrate. Sadik et al. [43] reported that no contribution of the TiAlN coating was found to tool life in milling Ti–6Al–4V under cryogenic cooling conditions.

Firstly, the tribological tests were performed to analyze the capability of the new coatings for the selection of coatings and for further tool wear tests; besides this, they can also provide information relevant to simulation jobs. Secondly, works on tribological tests relevant to cryogenic-assisted machining are few, and those addressing coatings are even fewer; as such, it is necessary to perform full-scale experiments to fill up the blank page in this field, especially for the Ti–6Al–4V alloy. Finally, it is important to effectively understand the tribological behaviors of the coatings and the workpiece, and particularly when cryogenic-assisted machining is being used. The lack of a state-of-art summary means this report contributes in this field.

A previous study [44] has shown the need to develop new tool materials, including coatings, to take full advantage of this cooling solution. Moreover, little is known about the tribological conditions at the tool–workpiece/chip interface when coated tools are used under cryogenic cooling conditions. This analysis will be performed on two cooling/lubrication strategies—LN₂, and traditional MWF consisting of an oil–water mixture—using both coated and uncoated pins in contact with a workpiece in Ti–6Al–4V titanium alloy, under several contact conditions. The instrument introduced by Rech et al. [3] is used as a specially designed tribometer to conduct the tribological tests, which leads to more reliable results compared to the classic pin-on-disk setup.

This study aims to expand the knowledge and understand the tribological conditions pertaining at the workpiece/chip interface when coated tools are used under cryogenic cooling conditions, so as to develop and select the most effective coatings (as confirmed by tribological tests) for machining Ti–6Al–4V alloys under cryogenic cooling conditions.

2. Materials and Experimental Set-Up

2.1. Materials

The pins were made of tungsten carbide with a cobalt content of 7 wt. % and a grain size of 0.8 μm. The hardness and the elastic modulus were determined using an MTS XP

Nanoindenter, and the corresponding values equalled 24.77 GPa and 839.07 GPa, respectively. The thermal conductivity of $41 \text{ W}\cdot\text{m}^{-1}\cdot\text{K}^{-1}$ was determined by MPTR (Modulated photothermal radiometry). The curvature and roughness of the pins were measured using the vertical profile projector Delta METROLOGIE VB12 series and a dynamic focusing microscope Alicona InfiniteFocus, respectively. The SEM images were taken by a high-resolution HRSEM (JEOL JSM 7610F). The work materials were Ti-6Al-4V bars, with an average microhardness of 3.4 GPa. The coatings CrN, AlCrN, M2 and M4 were prepared by an industrial deposition system KENOSISTEC-KS40V-113K12. CrN and AlCrN were the optimized monolayers, M2 and M4 were the multilayers made by the aforementioned monolayers with different numbers of interfaces and thicknesses. Additional information can be found in the reference [45].

2.2. Experimental Set-Up

The experimental set-up used in the tribological tests is shown in Figure 1. These tests, also called pi-on-bar tests, were conducted on a SOMAB T500 CNC lathe machine. A pin was mounted on the tribometer, and this tribometer was mounted on a piezoelectric dynamometer Kistler 9121 to measure the F_x , F_z and F_y forces (see Figure 1) acting in the pin. Then, a dynamometer was mounted in a VDI attachment connected to the turret of the CNC machine. The force signals were acquired by a NI cDAQ-9174 card at a sampling frequency of 2 kHz. Two cooling/lubrication strategies were used: LN_2 and traditional metal working fluid (MWF) consisting of an oil-water mixture, also called flood. This MWF was used since it is the reference MWF used in the industry. The mixture was prepared by diluting 7% of mineral oil from Blaser, reference B-Cool 755, in 93% of water (in volume). This lubricant is qualified for machining heat-resistant alloys such as titanium and nickel-based alloys. The LN_2 tank was placed on a balance to estimate the flow rate based on the weight variation. The tank was connected to an insulated flexible pipe to deliver the LN_2 to the nozzle. The pressure of LN_2 in the tank was 4 bar and the estimated flow rate was 2 L/min. Axial force generated by pressurized CO_2 gas inside a cylinder was used to generate the contact pressure between the pin and the bar. This precludes the low temperatures of the LN_2 affecting the forces signals; the dynamometer was covered in an insulation material. The nozzle was placed behind the pin in the direction of sliding, in order to reproduce the cooling/lubricant conditions applied in machining. The details of the LN_2 nozzle diameter and position are shown in Figure 2. They were optimized by Lequien [44], and correspond to the following: nozzle outlet diameter equal to 3 mm; distance between the nozzle and the pin equal to 2 mm; distance from nozzle to workpiece equal to 2 mm; the angle between the pin axes and the workpiece equal to 75° . The Ti-6Al-4V bar was pre-machined to generate a surface roughness similar to that of the chip surface in contact with the tool, which was considered to be equal to $0.1 \mu\text{m}$.

The apparent friction coefficient was determined using Equation (1):

$$\mu_{app} = \frac{F_t}{F_n} \quad (1)$$

where μ_{app} is the apparent friction coefficient, F_t is tangential force, and F_n is the normal force.

The tangential force F_t is equal to $\sqrt{F_z^2 + F_y^2}$, and the normal force F_n is equal to F_x . The term “apparent friction coefficient” used here differs from “interfacial friction coefficient”, which includes the adhesion at the pin-work material interface. Challen and Oxley [46] proposed a simple decomposition for the apparent friction coefficient, shown by Equation (2):

$$\mu_{app} = \mu_{loc} + \mu_{plast} \quad (2)$$

where μ_{loc} and μ_{plast} are the local adhesive and macroscopic parts, respectively.

Temperature was measured using a thermocouple type K inserted in a drilled hole from the bottom of the cylindrical body of the pin. The distance between the thermocouple and the contact surface between the workpiece and the pin was 1.53 mm [45].

The adhesion volume of the Ti-6Al-4V material to the pins was observed using optical microscope Keyence VHX 1000, then quantified using a dynamic focusing microscope Alicona InfiniteFocus [45].

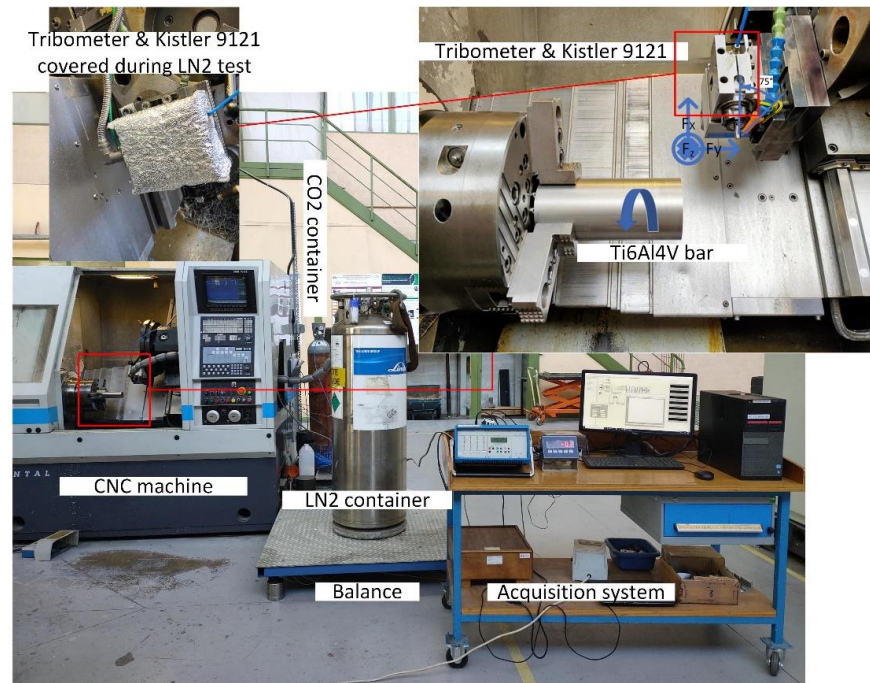


Figure 1. Experimental set-up used for tribological tests.



Figure 2. Nozzle position for tribological tests.

2.3. Determination of Contact Conditions in Machining of Ti-6Al-4V Alloy

As already mentioned above, the tribological tests should be conducted under the same contact conditions as those observed in metal cutting. Therefore, the chip sliding speed over the tool rake face and the tool–chip contact pressure should be calculated using

machining tests. Then, similar conditions should be applied between the pin and the Ti-6Al-4V in the tribological tests.

2.3.1. Determination of the Sliding Speeds between the Pin and the Ti-6Al-4V Bar

The sliding speed of the chip against the tool rake face is different from the cutting speed. As shown in Figure 3, a layer of material was separated from the workpiece by the action of the tool to form the chip. The ratio between the chip thickness and the uncut chip thickness, which is equal to the ratio between the cutting speed and the chip velocity, is called chip compression ratio (CCR), ζ , and it is given by Equation (3) [47]:

$$\zeta = \frac{h_1}{h} = \frac{V_c}{V_1} \quad (3)$$

where h and h_1 are uncut chip thickness (mm) and chip thickness, respectively. V_c and V_1 are the cutting speed and chip velocity (m/min), respectively. This equation shows that the chip velocity, V_1 , depends on both cutting speed and CCR. Since the CCR is usually greater than 1 (chips are generally thicker than the uncut chip thickness), the chip velocity is lower than the cutting speed.

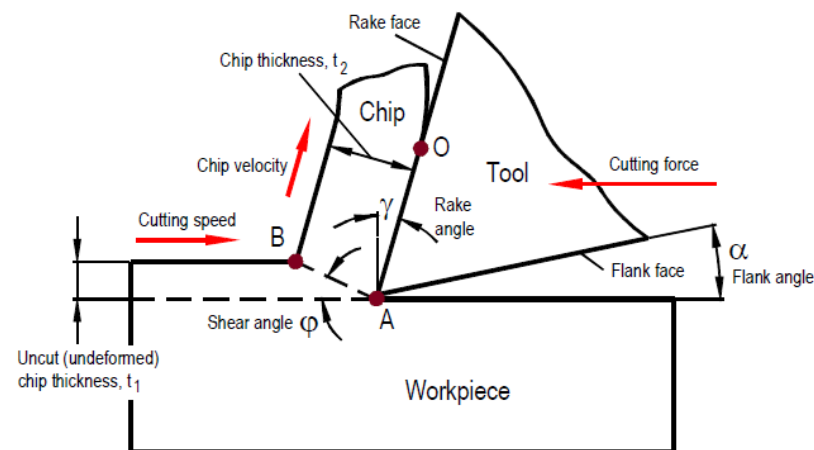


Figure 3. Single-shear plan model [48].

By analogy to the machining tests, in pin-on-bar tribological tests, the sliding velocity, V_s , is equal to the chip velocity, V_1 , in machining. Considering that the average CCR during the orthogonal cutting of Ti-6Al-4V alloy using uncoated cemented carbide tools is about 1.5 (Figure 4) [49], the sliding speeds can be determined for various cutting speeds using Equation (3), as listed in Table 2. The large range of cutting speeds can be used to determine the influence of this parameter on the tribological behaviour of coatings. It is noteworthy that the upper value of the cutting speed is a bit higher for machining Ti-6Al-4V alloy using commercial cemented carbide cutting tools. The main reason for using this value is to evaluate the tribological performance of the new coatings under more aggressive cutting conditions than those used today for commercial coated tools.

Table 2. Sliding velocities and correlated cutting speeds determined in tribological tests.

Cutting speed, V_c (m/min)	15	30	60	90	120	150
Sliding velocity, V_1 (m/min)	10	20	40	60	80	100

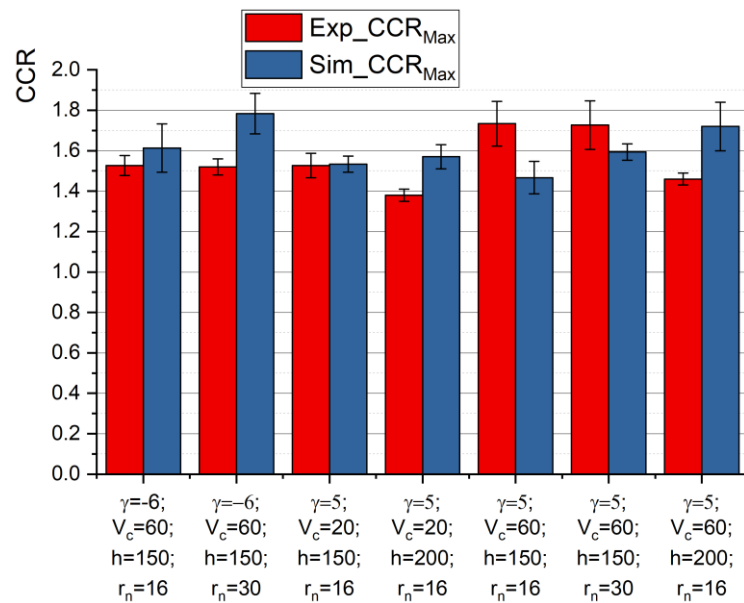


Figure 4. Chip compression ratio (CCR) in the orthogonal cutting of Ti-6Al-4V alloy using uncoated cemented carbide tools [49].

2.3.2. Determination of the Normal Force Acting in the Pins

Figure 5 shows the procedure used for determining the normal force to be applied into the pins in the tribological tests. The first step of this procedure consists of gathering the forces, CCR and the tool–chip contact lengths generated by the orthogonal cutting tests of Ti-6Al-4V alloy using cemented carbide tools. Based on the measured cutting (F_c) and thrust (F_t) forces, the normal force ($F_{n\gamma}$) to the tool rake face was calculated using the forces diagram for orthogonal cutting, shown in many publications [47,48]. Then, the average contact pressure ($P_{n\gamma}$) between the tool and the chip is calculated by dividing the normal force by the tool–chip contact area. The next step consists of calculating the normal force necessary to be applied to the pins ($F_{n,pin}$) to reach a contact pressure at the pin–workpiece interface (P_{pob}) equal to the contact pressure calculated in the cutting tests ($P_{n\gamma}$).

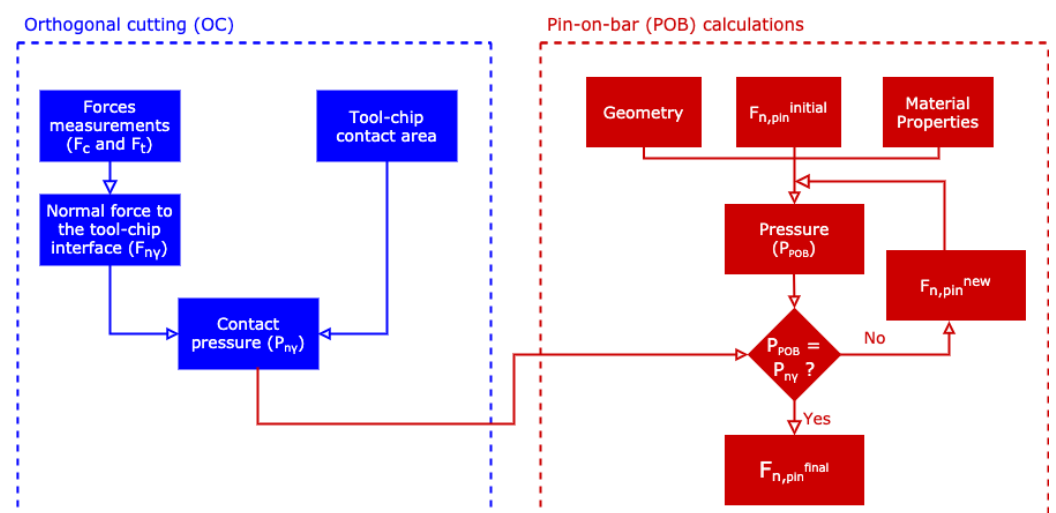


Figure 5. Flowchart of the procedure to determine the normal force to be applied to the pins.

Determination of the Contact Pressure in Machining of Ti-6Al-4V Alloy

Data from orthogonal cutting tests conducted by Outeiro et al. [50] were used in the procedure described above to calculate the normal forces acting on the pins during the tribological tests. This data are presented in Table 3, corresponding to two tests conducted

for two cutting speeds, keeping the other cutting regime parameters constant. The force diagram shown in Figure 6 was used to calculate the normal force applied to the tool rake face, $F_{n\gamma}$, using the measured cutting and thrust forces and the equations derived from this figure (Equations (4)–(6)) [48]. Then, the contact pressure was calculated by dividing the normal force $F_{n\gamma}$ by the tool–chip contact area (Equation (8)). This area is the product of the contact length l_c (Equation (7), taken from [48]) multiplied by the width of cut b .

$$R = \sqrt{F_c^2 + F_t^2} \tag{4}$$

$$F_{n\gamma} = R \cdot \sin\left[\frac{\pi}{4} + (\phi - \gamma)\right] \tag{5}$$

$$\phi = \tan^{-1}\left(\frac{\cos \gamma}{\zeta - \sin \gamma}\right) \tag{6}$$

$$l_c = h \cdot \zeta^{1.5} \tag{7}$$

$$P_{n\gamma} = \frac{F_{n\gamma}}{l_c b} \tag{8}$$

Under the cutting conditions listed in Table 3, the average contact pressure during the orthogonal cutting of the Ti–6Al–4V alloy for the selected cutting conditions is 1188 MPa. Therefore, a reference contact pressure of 1000 MPa is used in the tribological tests.

Table 3. Experimental data taken from the work of Outeiro et al. [50].

Test No.	Cutting Speed, V_c (m/min)	Uncut Layer Thickness, h (mm)	Width of Cut, b (mm)	Rake Angle, γ_n (°)	Flank Angle, α_n (°)	Edge Radius r_n (µm)	Cutting Force, F_c (N)	Thrust Force, F_t (N)	Chip Compression Ratio (CCR), ζ
1	55	0.15	4	6	7	30	1125	650	1.5
2	90	0.15	4	6	7	30	1100	630	1.4

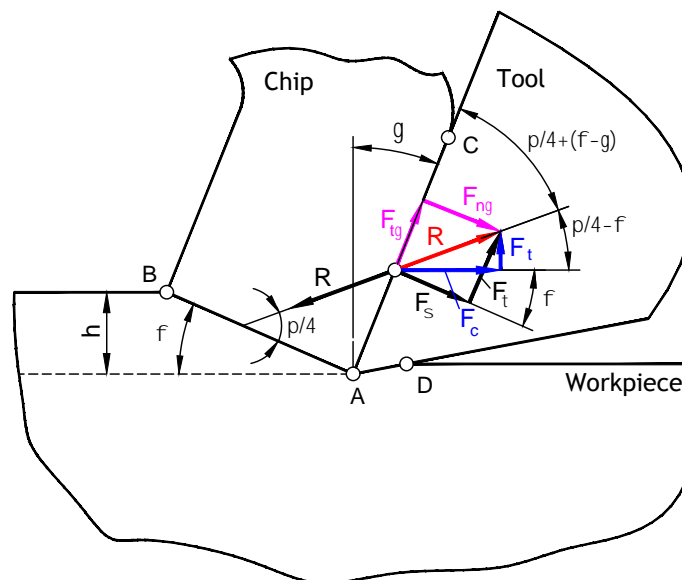


Figure 6. Force diagram of orthogonal cutting [48] (reproduced with permission from the author).

Determination of the Normal Force Acting in the Pins

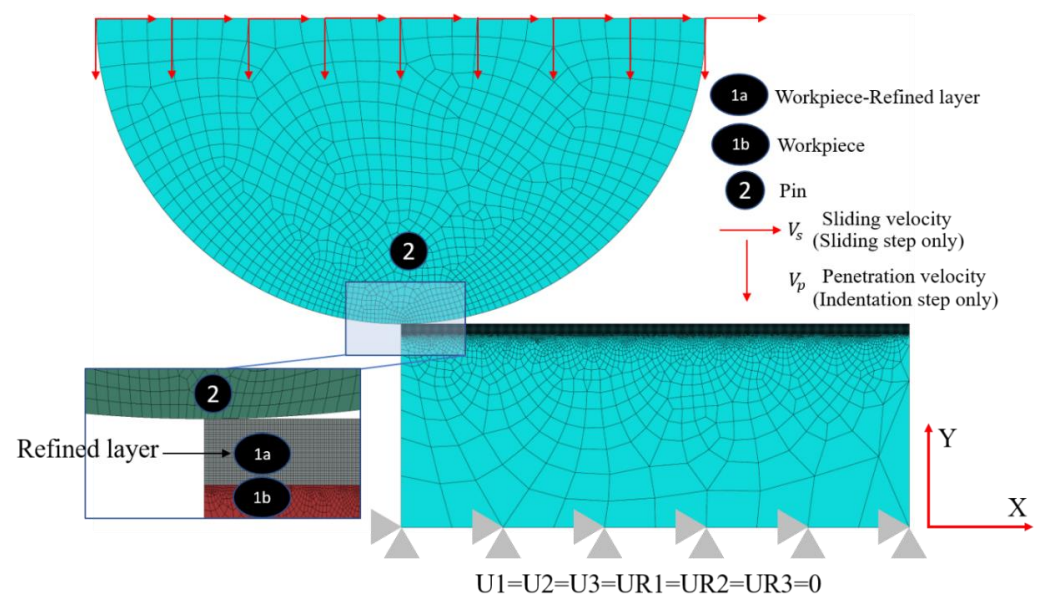
Since the geometries of cutting tools and pins are different, the values of the normal forces presented in Table 4 are not the same as those to be applied in tribological tests for the same contact pressures. Therefore, the normal force acting in the pins should be calculated.

Table 4. Contact forces and pressures used in the pin-on-bar model [51].

Test No.	Resultant Force R (N)	Contact Length, l_c (mm)	Normal Force, $F_{n\gamma}$ (N)	Contact Pressure, P (MPa)
Test 1	1299	0.276	1252	1136
Test 2	1268	0.248	1233	1240

Initially, two analytical models of the pin-on-bar test were developed using the Hertz theory for both elastic and elastoplastic contact. However, these models considered only the indentation in a static contact between two spheres, so the sliding was neglected, which does not exactly represent the physical phenomenon occurring in the pin-on-bar test. Therefore, an inverse approach consisting of conducting numerical simulations of the pin-on-bar tests was applied by varying the normal force until the contact pressure at the pin-workpiece interface (P_{pob}) was equal to the pressure calculated from the cutting tests ($P_{n\gamma}$).

A model of the pin-on-bar test was developed and simulated using the Abaqus FEA (implicit) software (Abaqus 2022). This model is shown in Figure 7, where the pin comprises uncoated cemented carbide with a radius of 6 mm sliding over a flat workpiece made of Ti-6Al-4V, with a rectangular shape of 10 mm length and 4 mm height. The workpiece was fixed at its bottom side and the pin was allowed to slide over the top surface of the workpiece in the X-direction at a constant speed (the sliding speed). Amongst the sliding speeds shown in Figure 4, five of them were used in the simulations of pin-on-bar: 10, 20, 40, 60 and 80 m/min. Due to the convergence issues, the application of a force to the pin was replaced with a displacement imposed on the pin in the direction normal to the workpiece surface until reaching the desired normal force.

**Figure 7.** Model of the pin-on-bar tribological test.

The materials of the workpiece and pin were considered as isotropic. The elastic properties of the Ti-6Al-4V alloy were taken from Cheng et al. [52], while the elastic properties of the pin were obtained from several studies found in the literature [53–55]. The Johnson–Cook constitutive model [56] without the temperature term is used to represent the plastic behavior of the Ti-6Al-4V alloy, as described by Equation (9):

$$\bar{\sigma} = (A + B \cdot \epsilon^n) \left[1 + C \cdot \ln \left(\frac{\dot{\epsilon}}{\dot{\epsilon}_0} \right) \right] \quad (9)$$

where the first term represents the strain hardening effects, and the second term the strain-rate effect. ε_p and $\dot{\varepsilon}$ (equal to 0.05 s^{-1}) are the plastic strain and strain-rate, respectively. The coefficients A , B , C and n of this plasticity model were determined by Cheng et al. [52] via quasi-static and dynamic (different strain-rates) compression tests conducted over samples from the same bar used in the tribological tests. The mechanical properties of both the workpiece and pin are listed in Table 5.

Table 5. Mechanical properties used in the pin-on-bar model taken from Cheng et al [52].

	Ti-6Al-4V	WC
Density (Kg/m ³)	4420	13,967
Elastic modulus (GPa)	114	627.5
Poisson's ratio	0.31	0.25
Coefficients of the constitutive model	$A = 812; B = 844$ $C = 0.015; n = 0.261$	----

The friction coefficient in relation to the sliding speed was taken from the work of Courbon et al. [57], obtained for the same pin and workpiece materials using similar tribological tests. This friction coefficient can be represented by the following equation:

$$\mu = 0.359 - 0.042 \cdot \ln(V_s) \quad (10)$$

where V_s is the sliding speed.

The simulation was divided into two steps: indentation and sliding. In the indentation step, the pin penetrated to a given depth in the workpiece to establish the suitable average contact pressure. Then, in the sliding step, the pin slid 10 mm over the workpiece's top surface in the X-direction at a constant sliding speed. After the simulation, the contact pressure was extracted from the model and compared with that obtained by orthogonal cutting (see procedure in Figure 5). If they were different, the penetration depth was modified, and a new simulation was performed. This procedure was applied until both contact pressures were similar, and consequently the normal force acting in the pin was obtained.

Both pin and workpiece were meshed with a four-node plane stress element type (CPS4R). A thin layer of 0.2 mm was placed on top of the workpiece to refine the mesh. Maximum element sizes of 1 mm and 0.5 mm were used for the pin and workpiece, respectively. To determine the minimum element size, the influence of element size on the results was studied. In addition, since the model is a simplification of the pin-on-bar geometry (initial bar diameter is equal to 80 mm), the influence of the equivalent radius used in the Hertz theory [58,59] is also presented below. After this, the simulations were conducted for the five sliding speeds mentioned above.

Furthermore, the minimum element size, the equivalent radius and the different sliding speeds were consulted to determine their influences on the determination of the normal force.

The tested minimum element sizes are presented in Table 6, and the results are depicted in Figures 8 and 9. The largest combination of minimum element sizes for the pin and workpiece, depicted as Pin (P)-Workpiece (W) (200 μm for the pin and 40 μm for the workpiece), manifested the largest discrepancy in normal force and contact stress compared to the other three element sizes. The average contact stresses are 1059 MPa, 1003 MPa, 907 MPa and 781 MPa for the mesh sizes 25P-5W, 50P-10W, 100P-20W and 200P-40W, respectively. The two finest combinations of minimum element size, 25P-5W and 50P-10W, generated similar normal forces of 439 N and 436 N, respectively. Considering the accuracy of the results and the computational time, the combination of minimum element sizes 50P-10W was chosen for the simulations to calculate the normal force acting in the pins for different sliding speeds.

Table 6. Minimum element sizes of the tested pins and workpieces.

	Minimum Element Size (μm)			
	Mesh 200P-40W	Mesh 100P-20W	Mesh 50P-10W	Mesh 25P-5W
Pin	200	100	50	25
Workpiece	40	20	10	5

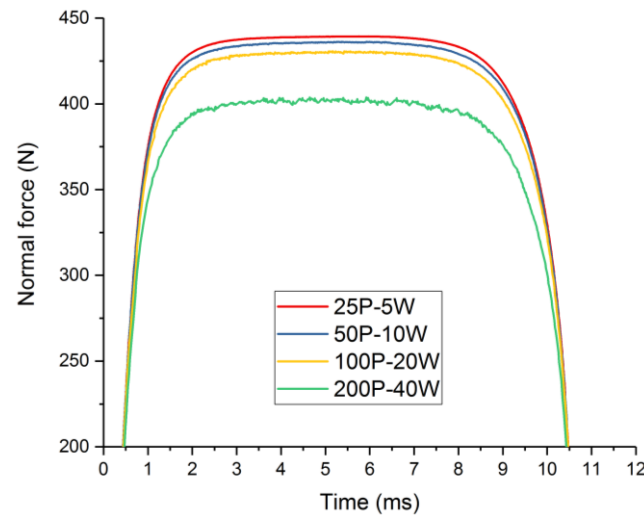


Figure 8. Normal forces across time for several minimum element sizes.

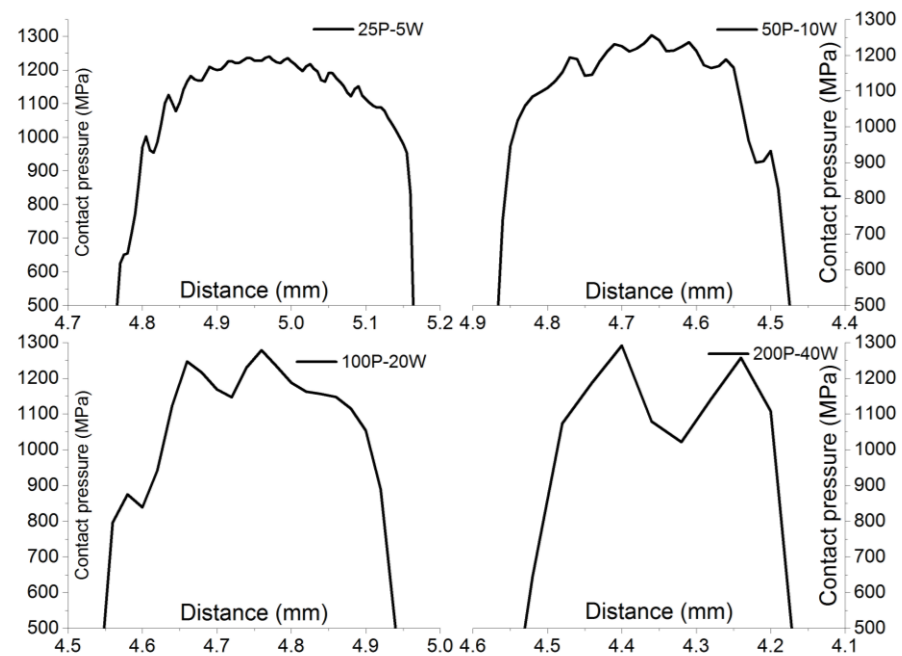


Figure 9. Contact stress distribution according to the minimum element size.

The equivalent radius (R_{eq}) was calculated using Equation (11), where R_{pin} and R_{work} are the radius of the pin and workpiece, respectively. The equivalent radius (R_{eq}) values calculated considering a bar with an initial diameter of 80 mm and a final one of 56 mm are listed in Table 7. The normal force and the contact pressure distribution calculated based on R_{eq} are illustrated in Figures 10 and 11, respectively. The normal forces for these three different radii corresponding to the original pin radius of 6 mm, and the equivalent pin radii of 5.2 mm and 5 mm, are 436 N, 414 N and 406 N, respectively. The distributions of

the contact stresses are almost the same. Since the error did not exceed 7%, we could use the original radius of 6 mm to simulate a real pin-on-bar test.

$$R_{eq} = \frac{1}{\frac{1}{R_{pin}} + \frac{1}{R_{work}}} \tag{11}$$

Table 7. Equivalent radius (R_{eq}) values calculated considering a bar with an initial diameter of 80 mm and a final one of 58 mm.

Workpiece Radius, R_{work} (mm)	40 (Initial)	28 (Final)
Pin radius, R_{pin} (mm)	6	6
Equivalent pin radius, R_{eq} (mm)	5.2	5

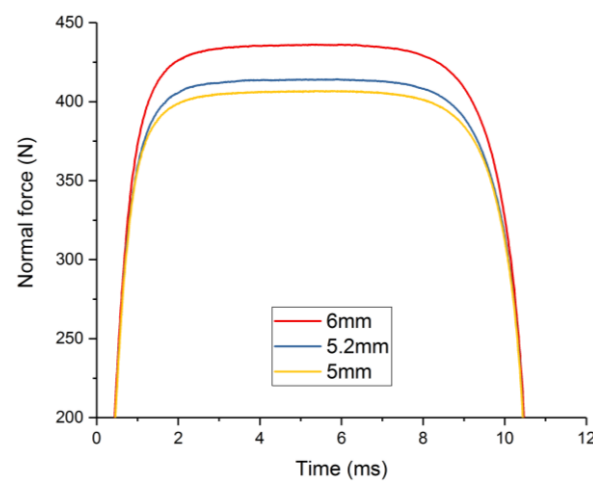


Figure 10. Normal forces across time for different pin radii.

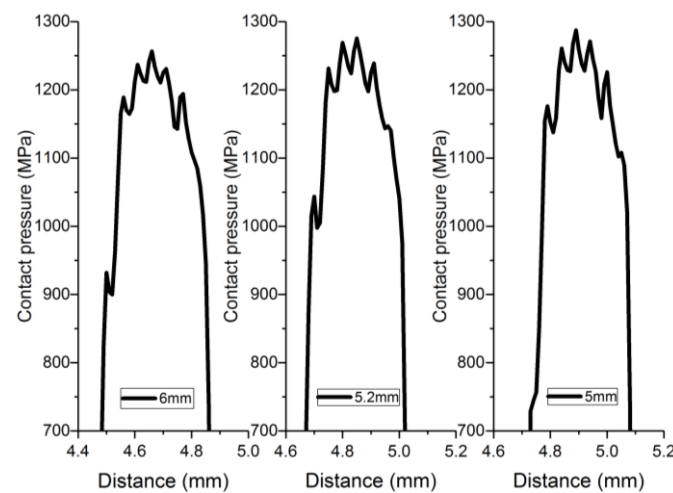


Figure 11. Contact stress distribution for different pin radii.

The influence of sliding speeds was studied by using five sliding speeds to determine the normal forces able to reproduce a reference average contact pressure of around 1000 MPa, as determined by orthogonal cutting. The results are shown in Figures 12 and 13. The maximum contact pressures are closed to 1260 MPa, with an average pressure of 989 MPa. These figures also show that the sliding speed had a small effect on the normal force and contact pressure. The normal force varied from 423 N for the lowest speed of 10 m/min to 437 N for the highest speed of 100 m/min, corresponding to a variation of

14 N. The average contact pressure varied from 975 MPa for the lowest speed of 10 m/min to 1006 MPa for the highest speed of 100 m/min, corresponding to a variation of 31 MPa.

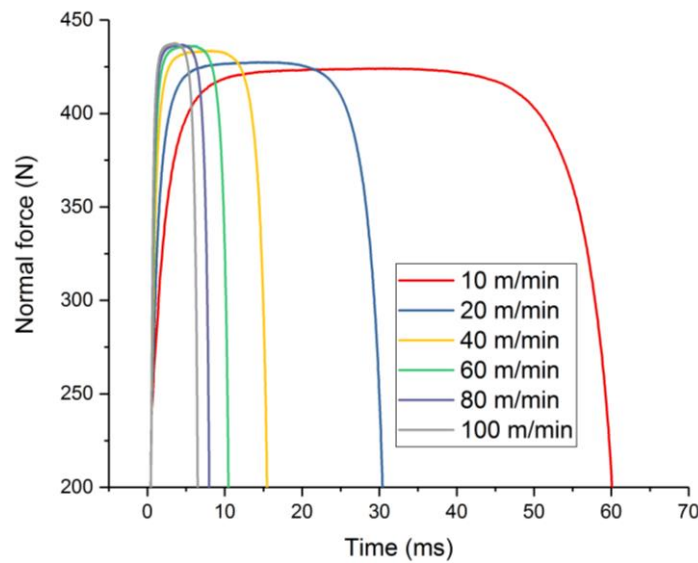


Figure 12. Normal forces across time for several sliding speeds.

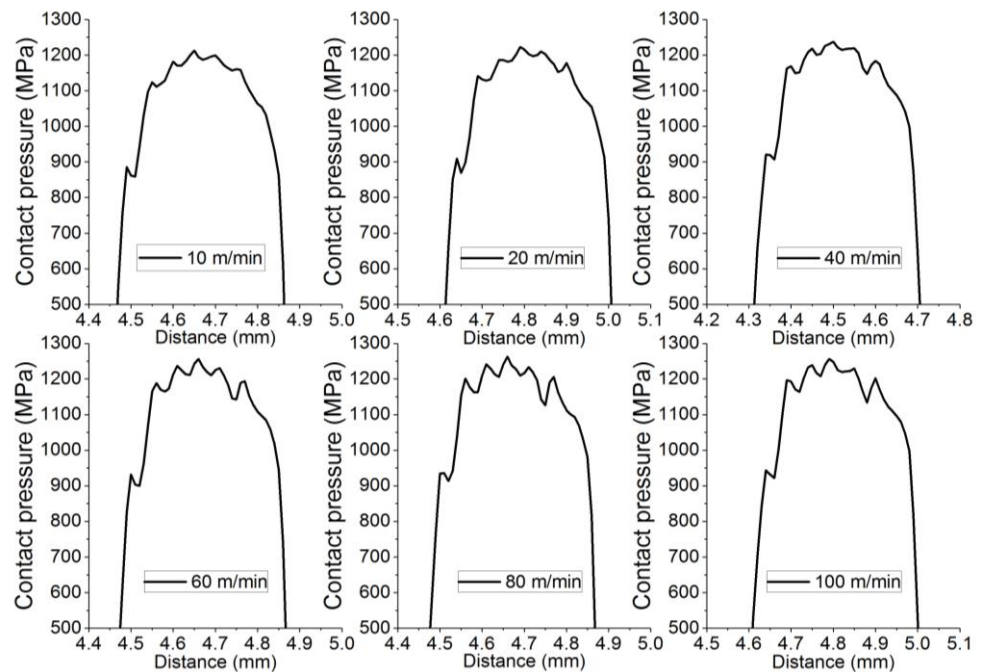


Figure 13. Contact stress distribution for several sliding speeds.

Based on these analyses, it was decided to apply a normal force of 300 N during the tribological tests, corresponding to an average contact pressure of 872 MPa.

2.4. Surface Roughness of the Pins

The roughness of the pins was measured after the depositions using the dynamic focusing microscope *Alicona InfiniteFocus*. The results are shown in Figures 14–16. The average roughness of uncoated and coated pins varied from 0.5 to 0.71 μm , the root mean square roughness varied from 0.63 to 0.91 μm , and the maximum height varied from 3.64 to 6.21 μm . The coatings slightly increased the roughness of the pins according to R_a and R_q ; although the coatings followed the surface topography of the substrate, this may

be due to the triangular tips of the coatings. The roughness values of the AlCrN monolayer and the M2 and M4 multilayers were almost the same, because their top layers were both an AlCrN monolayer. The maximum height values reveal that AlCrN was rougher than the other coated pins. The SEM images of the coated pins are presented in Figure 17. The EHT (extra high tension) was 15 kV for CrN, M2 and M4, and 5 kV for AlCrN; the WD (working distance) was 35 mm for CrN, M2 and M4, and 15.3 mm for AlCrN; the magnification was $\times 500$ for all. This figure shows that the AlCrN monolayer had more random small particles on its surface compared to the other coatings. Indeed, the M2 and M4 multilayers contained fewer particles than the AlCrN and CrN monolayers; the particles relatively homogenous among all the coatings. This may be due to the unstable micro-arc phenomenon that occurred during the deposition of the AlCrN monolayer. The quantity and distribution of these small particles justifies the surface roughness values observed between different coatings.

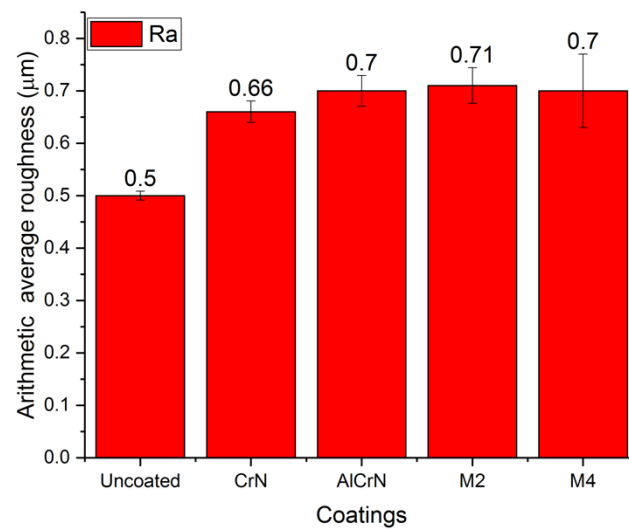


Figure 14. Average roughness (R_a) of the pins with different coatings.

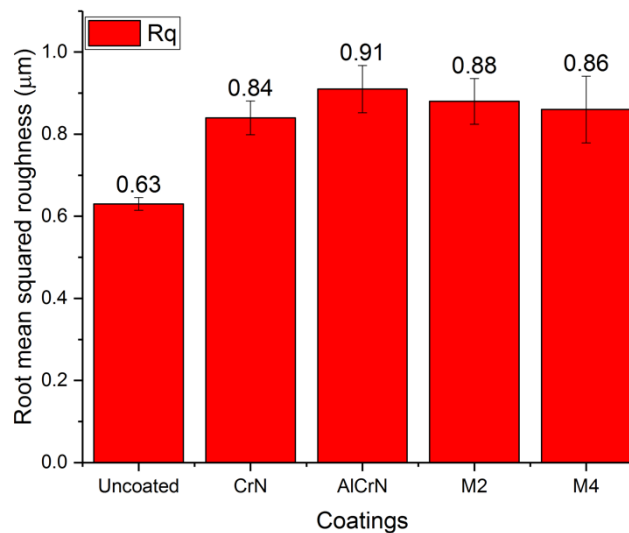


Figure 15. Root mean square roughness (R_q) of the pins with different coatings.

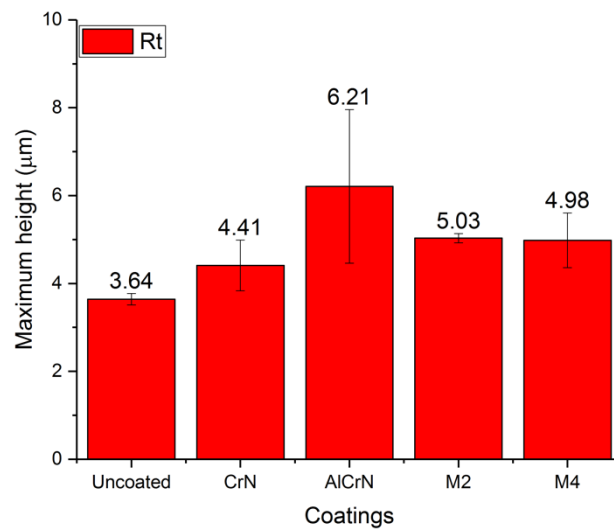


Figure 16. Maximum height of the roughness profile (R_t) of the pins with different coatings.

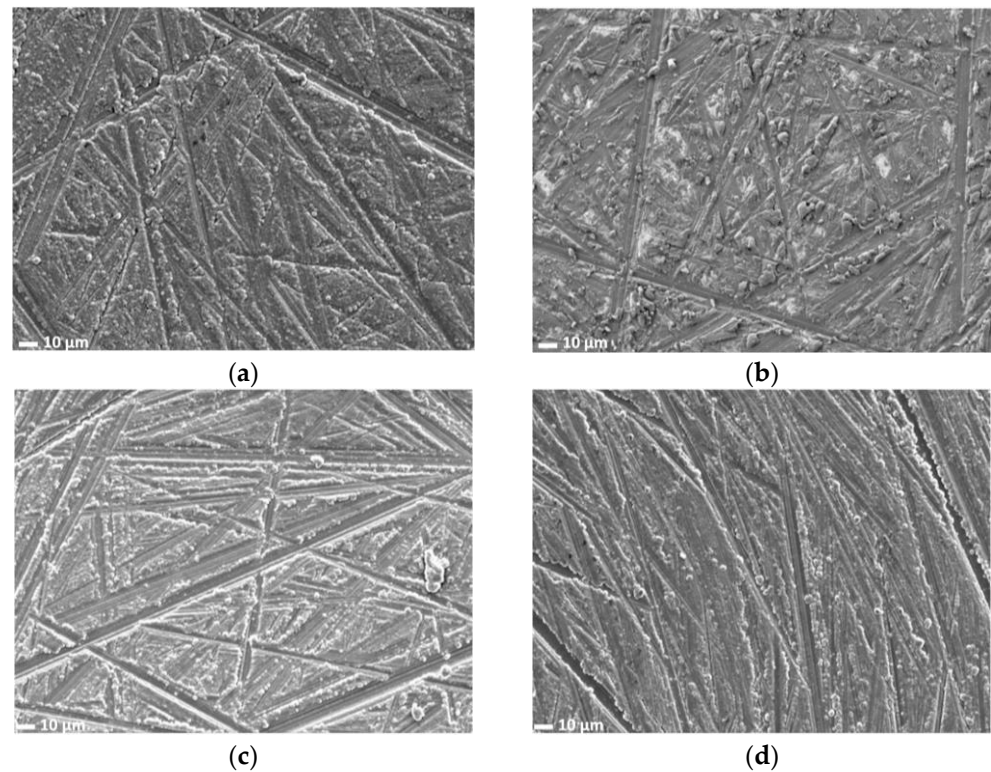


Figure 17. SEM images of the surface morphology of CrN- (a), AlCrN- (b), M2- (c), and M4 (d) -coated pins.

2.5. Design of Experiments

The Design of Experiments (DoE) comprised the three factors (sliding speed, coating type and type of MWF) and several levels listed in Table 8. The contact pressure was not included in this DoE, since at this stage we assumed a constant contact pressure equal to 872 MPa. Each condition was tested twice (one repetition), corresponding to a total of 120 tests. The outputs were the normal and tangential forces, the friction coefficient, and the volume of the layer of build-up of Ti-6Al-4V alloy in the pins. Temperature was also measured (twice), but only for the sliding speed of 60 m/min. The measured average normal force applied on these tests was 316 N, with an average contact pressure of 877 MPa. The maximum normal force applied was 393 N, with an average contact

pressure of 971 MPa. The minimum normal force applied was 266 N, with an average contact pressure of 839 MPa.

Table 8. Factors and levels used in the multilevel factorial DoE.

Factors	Levels
Sliding speed (m/min)	10, 20, 40, 60, 80 and 100
Coating Type	No coating (uncoated pin), CrN, AlCrN, M2 and M4
MWF Type	LN ₂ and mixture of oil–water

To evaluate the influence of the contact pressure, 12 additional tests were performed by applying a normal force of 1400 N to the pins, corresponding to an average contact pressure of 1329 MPa, calculated using the numerical model presented previously. These additional tests are shown in Table 9. The sliding distance for each tribological test was equal to 4 m.

Table 9. Additional tests for an average contact pressure of 1329 MPa.

No.	Sliding Speed (m/min)	Coating Type
1	10	Uncoated
2	20	Uncoated
3	40	Uncoated
4	60	Uncoated
5	80	Uncoated
6	100	Uncoated
7	20	Uncoated
8	60	Uncoated
9	100	Uncoated
10	20	M2
11	60	M2
12	100	M2

3. Results and Discussion

3.1. Results of the Tribological Tests

Based on the tangential and normal forces obtained from the tribological tests, the apparent friction coefficient was determined. Figure 18 shows the friction coefficient as a function of the sliding speed for different coatings, for both MWF (flood and LN₂) and for an average contact pressure of 872 MPa. This figure shows that the apparent friction coefficient decreased as the sliding speed increased until about 60–80 m/min, then it increased as the sliding speed increased up to 100 m/min. Similar results were also obtained by Meier et al. [21] using an in-process (cutting) open tribometer to determine the friction coefficient between the Ti–6Al–4V alloy and 6 mm-diameter pins coated with an AlTiN coating, using several pin axial (normal) forces (between 5 N and 400 N), and under dry and lubricated (oil) conditions. Similar to the present work, they also found that the apparent friction coefficient showed a minimum value for intermediate sliding speeds when 100 N of normal force was applied. According to Meier et al. [21], the increase in the friction coefficient with higher sliding speeds may be due to the higher shear forces at higher relative speeds, and a stronger adhesion of the workpiece material to the pins. This strong adhesion at higher speeds was observed in the present tribological tests, as shown in Figure 19. This figure shows a strong increase in the volume of the layer of build-up of the Ti–6Al–4V alloy in the pins with sliding speeds greater than 60–80 m/min, under both flood and LN₂ coolant/lubricant conditions. Nevertheless, the uncoated pin seemed to present a lower adhesion of Ti–6Al–4V alloy under LN₂ cooling conditions (Figure 19b), which can be explained by its lower surface roughness (Figure 14). This volume was higher when LN₂ was applied, compared to the flood, due to the non-existent lubricant action of LN₂ compared to the flood. The coating type does not have a significant influence on

the friction coefficient, as for each sliding speed, the variance in the friction coefficient was within about 0.05 for coated and uncoated pins under the flood condition, regardless of the coating type. The low variance may originate from the different roughnesses of the pins, but the relevance of this is low (Figures 14–16). Under the LN₂ condition, relatively higher variances in both the friction coefficient and the adhesion volume were presented for different coating types; these may be due to the different tribological mechanisms for each coating type. The contact conditions and the degrees of delamination of the coating from the pins are different, both of which need to be studied further.

As far as the average contact pressure is concerned, increasing the pressure from 872 MPa to 1329 MPa reduces the apparent friction coefficient, as shown in Figure 20 for uncoated and coated pins (M2) and both MWF. In particular, the apparent friction coefficient decreased monotonically with the sliding speed when a higher pressure was used and for both MWFs. Similar results were also obtained by Meier et al. [21]. However, this reduction in the apparent friction coefficient was not followed by a reduction in the volume of the layer of build-up of Ti-6Al-4V alloy in the pins; in fact, the opposite was observed, as shown in Figure 21.

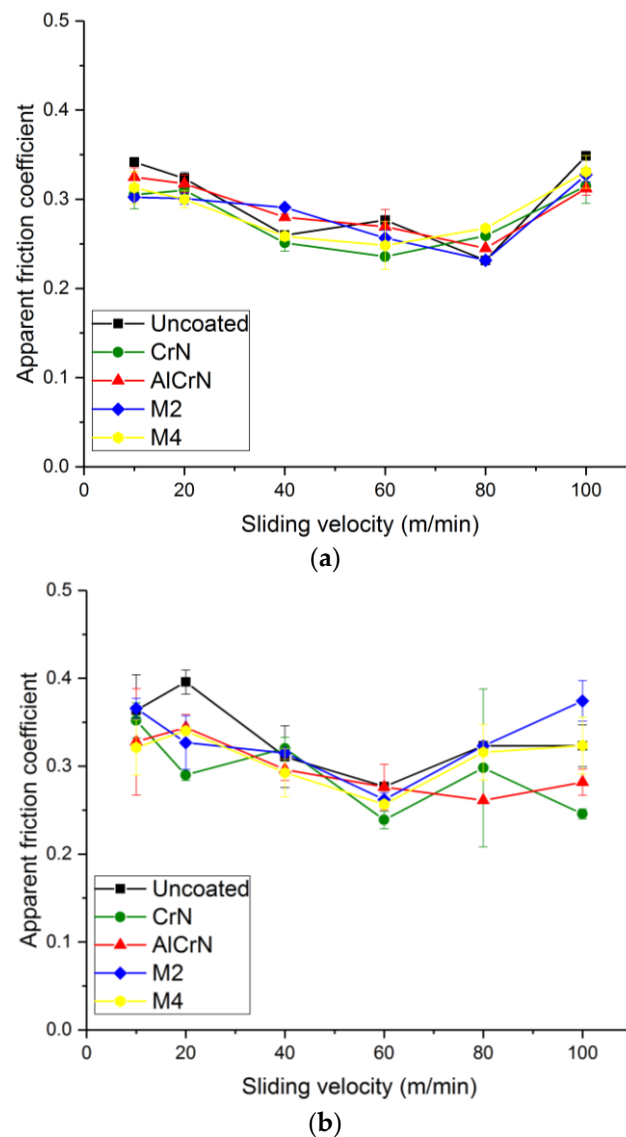
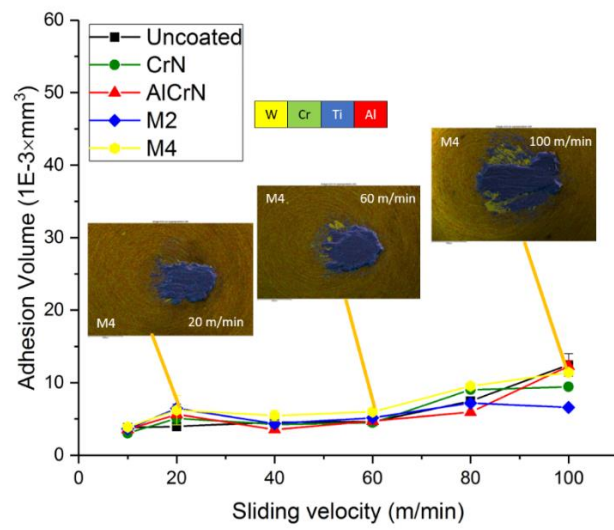
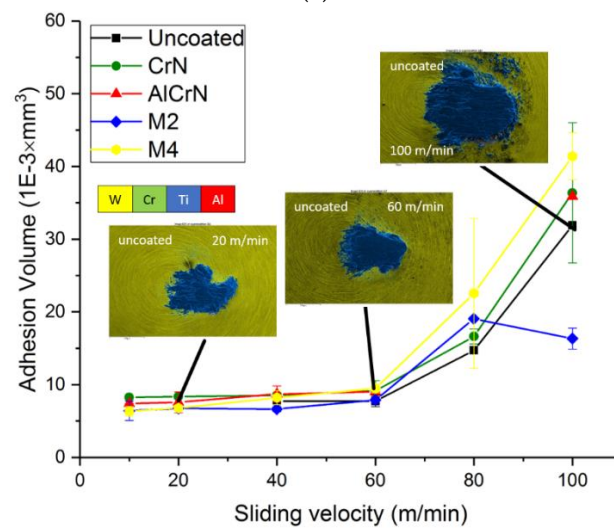


Figure 18. Apparent friction coefficient according to sliding speed and for different coatings, for (a) flood and (b) LN₂ (average contact pressure of 872 MPa).

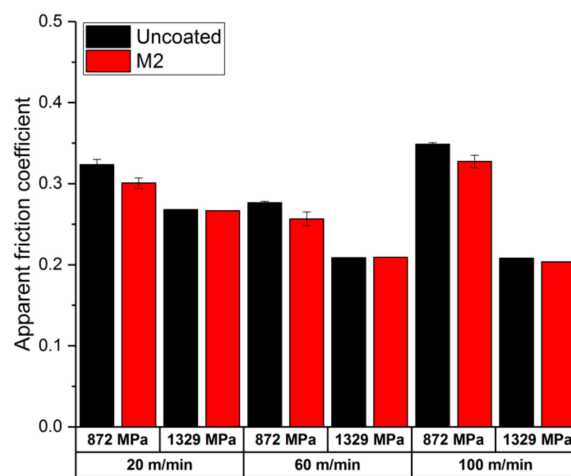


(a)



(b)

Figure 19. Volume of layer of build-up of Ti-6Al-4V alloy in the pins according to the sliding speed and for different coatings, for (a) flood and (b) LN₂ (average contact pressure of 872 MPa).



(a)

Figure 20. Cont.

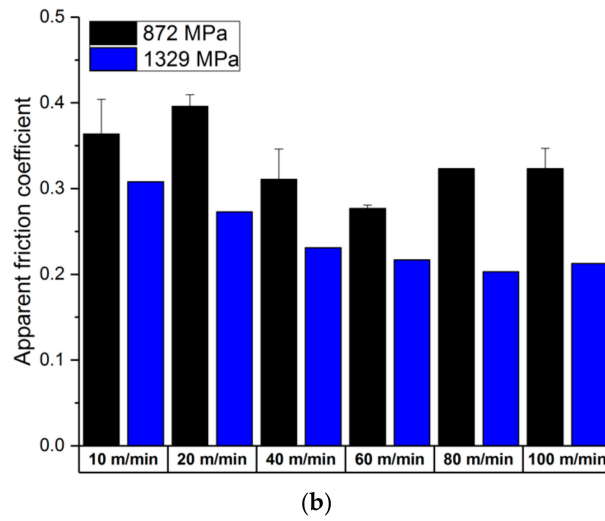


Figure 20. Apparent friction coefficient according to the sliding speed for two average contact pressures (872 MPa and 1329 MPa), for (a) flood conditions using coated (M2) and uncoated pins, and (b) for LN₂ conditions using uncoated pins.

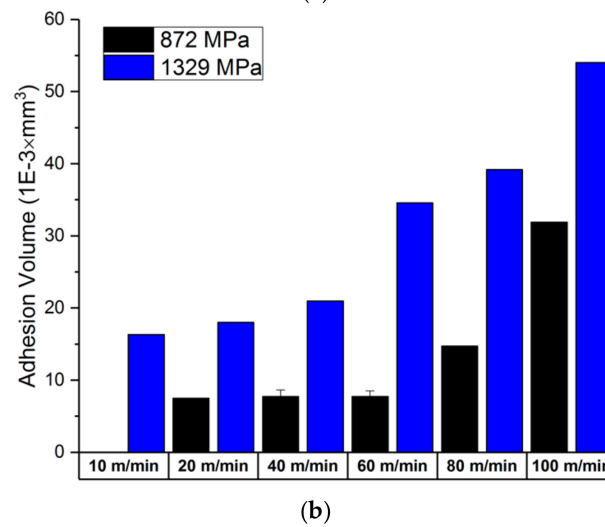
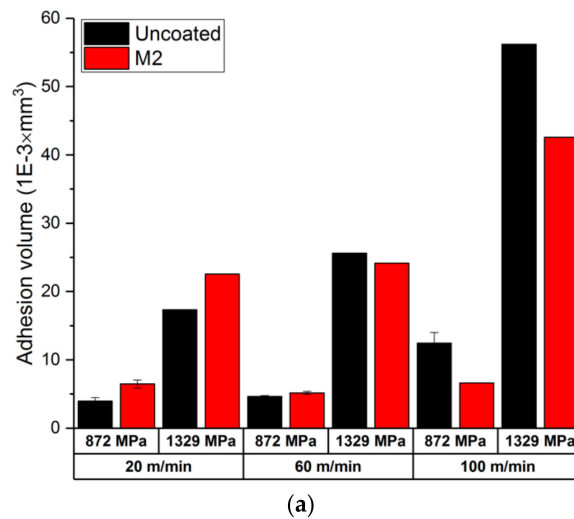


Figure 21. Volume of layer of build-up of Ti-6Al-4V alloy in the pins as a function of the sliding speed for two average contact pressures (872 MPa and 1329 MPa), for (a) flood conditions using coated (M2) and uncoated pins and (b) for LN₂ conditions using uncoated pins.

The apparent friction coefficients between the uncoated pins and the Ti6-Al-4V alloy with an average contact pressure of 1329 MPa and under LN₂ cooling conditions were compared with those obtained by Courbon et al. [57], as shown in Figure 22 for different sliding speeds. The present work yielded apparent friction coefficients about 20% higher than those found by Courbon et al. [57]. This difference may be due to the different contact conditions (pressure, temperature, etc.) between the present tribological tests and those performed by Courbon et al. [57], because the LN₂ (including the flow characteristics), pin diameter and normal forces applied were not the same in the present tribological test. Despite these differences, both curves of the apparent friction coefficient followed the same trend in relation to sliding speed.

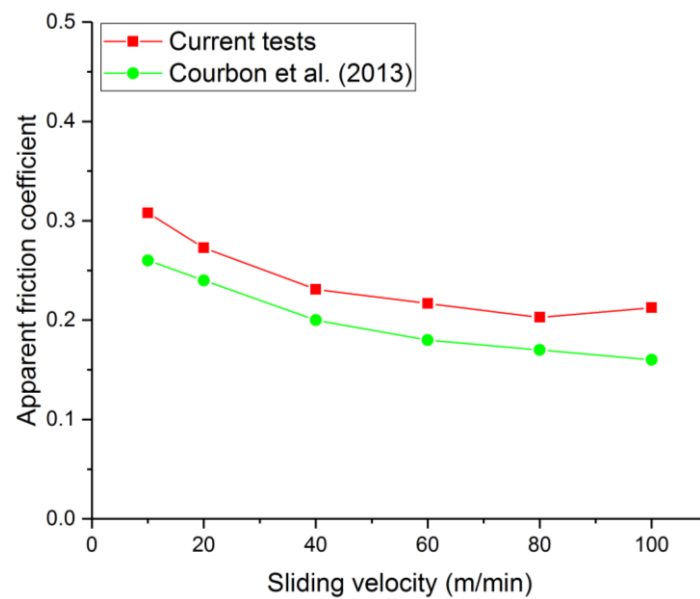


Figure 22. Apparent friction coefficient as a function of the sliding speed obtained in the current tribological tests and by Courbon et al. [57] (uncoated pin; average contact pressure of 1329 MPa; LN₂ cooling).

As far as the coating is concerned, and regardless of which MWF was used in the tribological tests, Figures 18 and 19 show no clear effects of the coating on the apparent friction coefficients and volumes of the built-up layer of Ti-6Al-4V alloy in the pins, respectively. As far as the temperature in the pins is concerned, some differences between the coatings can be seen in Figure 23. This figure shows the temperatures in the pins with different coatings and for both MWFs, at an average contact pressure of 872 MPa and a sliding speed of 60 m/min. These temperatures were extracted from the curves of the temperature as a function of time, acquired during the tribological tests, and correspond to a cutting time of 3.5 s for all the coatings shown in Figure 23.

This temperature was higher and more positive for flood conditions when compared to LN₂ cooling, wherein the temperature was negative. Moreover, this temperature was higher for uncoated pins, regardless of the MWF. The presence of a lower temperature in the pins depended on the coating and MWF used in the tribological tests. Under flood conditions, the lowest temperature was observed for the AlCrN coating, followed by M2 and M4. Under LN₂ cooling conditions, the lowest temperature was observed for the M4 coating, followed by CrN, AlCrN and M2. Nevertheless, from the thermal perspective, the coated pins performed better than the uncoated ones, because their temperatures were lower than that of the uncoated one. This means that the heat generated by the friction conducted to the pins would be lower in coated pins when compared to uncoated ones.

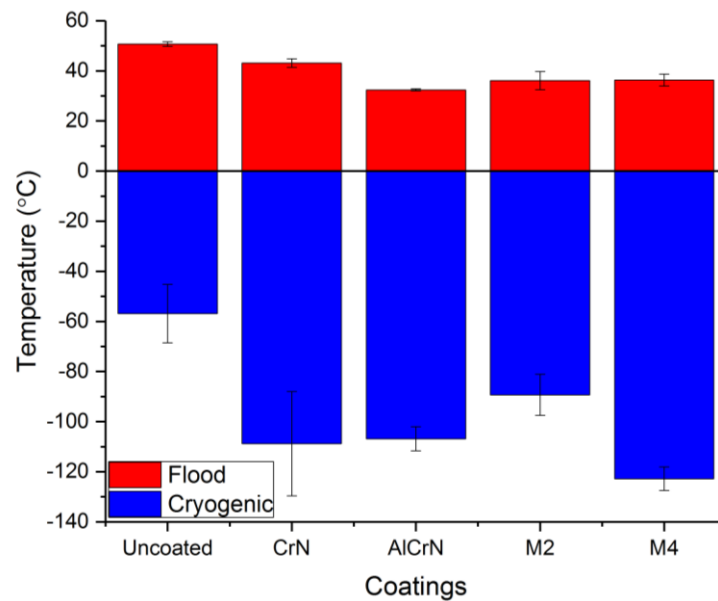


Figure 23. Temperature in the pins with different coatings (average contact pressure of 872 MPa and a sliding speed of 60 m/min).

3.2. DoE Analysis and Discussion

In this section, an analysis of the DoE presented in Section 2.5 is performed, with the following objectives:

1. To identify the relevant factors affecting the apparent friction coefficients and the volume of built-up layer of Ti-6Al-4V alloy in the pins;
2. To determine the influence of these relevant factors on the apparent friction coefficient and the volume of the built-up layer of Ti-6Al-4V alloy in the pins.

This DoE analysis was performed using the *Minitab*TM statistical software (Minitab® 20). The first step was to identify the significant factors affecting the apparent friction coefficient and the volume of the built-up layer of Ti-6Al-4V alloy in the pins, as well as their interactions, using Pareto analysis. As shown in Figure 24, the significant factors are the type of MWF (flood vs. LN₂), the sliding speed, and their interaction. The type of coating showed no significance, confirming what was already mentioned in the previous section. As shown in Figures 18 and 19, the apparent friction coefficient varied within 0.05 under flood conditions, and within 0.1 under cryogenic conditions, for all pins. Similar small variations can be found in the built-up layer of Ti-6Al-4V.

Figure 25 shows a graphical representation of the influence of the significant factors (MWF, sliding speed and their interactions) on the apparent friction coefficient. Figure 25a shows that the apparent friction coefficient was higher for cryogenic (LN₂) cooling when compared to flood conditions. This can be explained by the fact that no lubricant was used during cryogenic cooling with LN₂. This figure also shows a decrease in the apparent friction coefficient with sliding speed up to 60 m/min, followed by an increase up to 100 m/min. This confirms the previous results, and this behavior can be attributed to the increase in the adhesion after 60 m/min. Figure 25b shows the interaction between the type of MWF and the sliding speed. This figure shows that, for most of the sliding speeds (except for 100 m/min), the apparent friction coefficient was higher for cryogenic (LN₂) cooling compared to flood conditions.

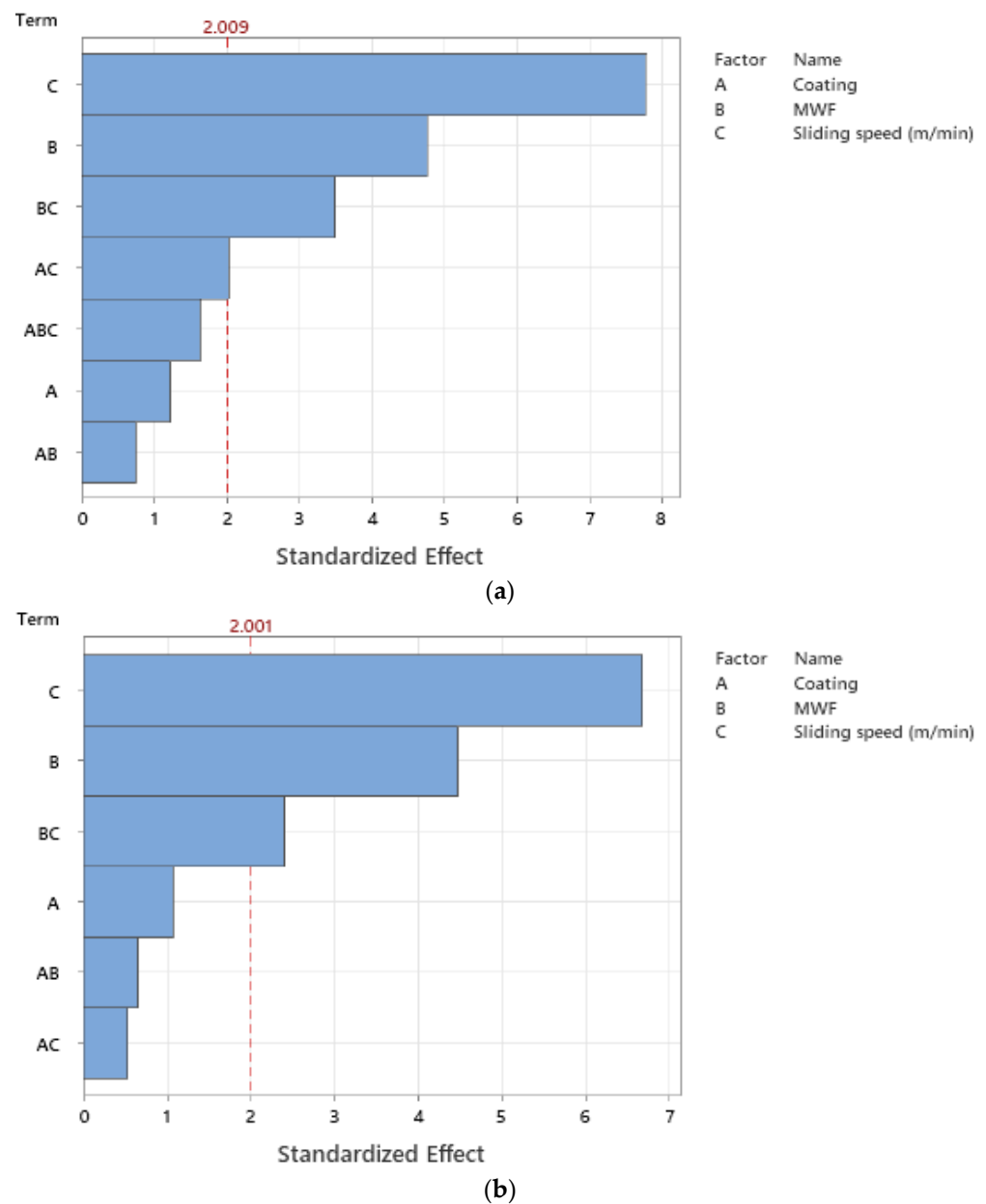


Figure 24. Pareto analysis of the factors affecting the (a) apparent friction coefficient and (b) the volume of the built-up layer of Ti-6Al-4V alloy in the pins.

Figure 26 shows a graphical representation of the influence of the significant factors on the volume of the built-up layer of Ti-6Al-4V alloy in the pins. This volume can be used to estimate the degree of adhesion of Ti-6Al-4V alloy in the pins. Figure 26a shows that the adhesion was higher for cryogenic (LN₂) cooling when compared to flood conditions. Again, this can be explained by the fact that no lubricant was used during cryogenic cooling with LN₂. This figure also shows that adhesion was almost constant up until a sliding speed of 60 m/min, followed by a fast increase in adhesion beyond 60 m/min until 100 m/min. Figure 26b shows that adhesion was higher under cryogenic (LN₂) cooling when compared to flood conditions, regardless of the sliding speed, which confirms the previous results.

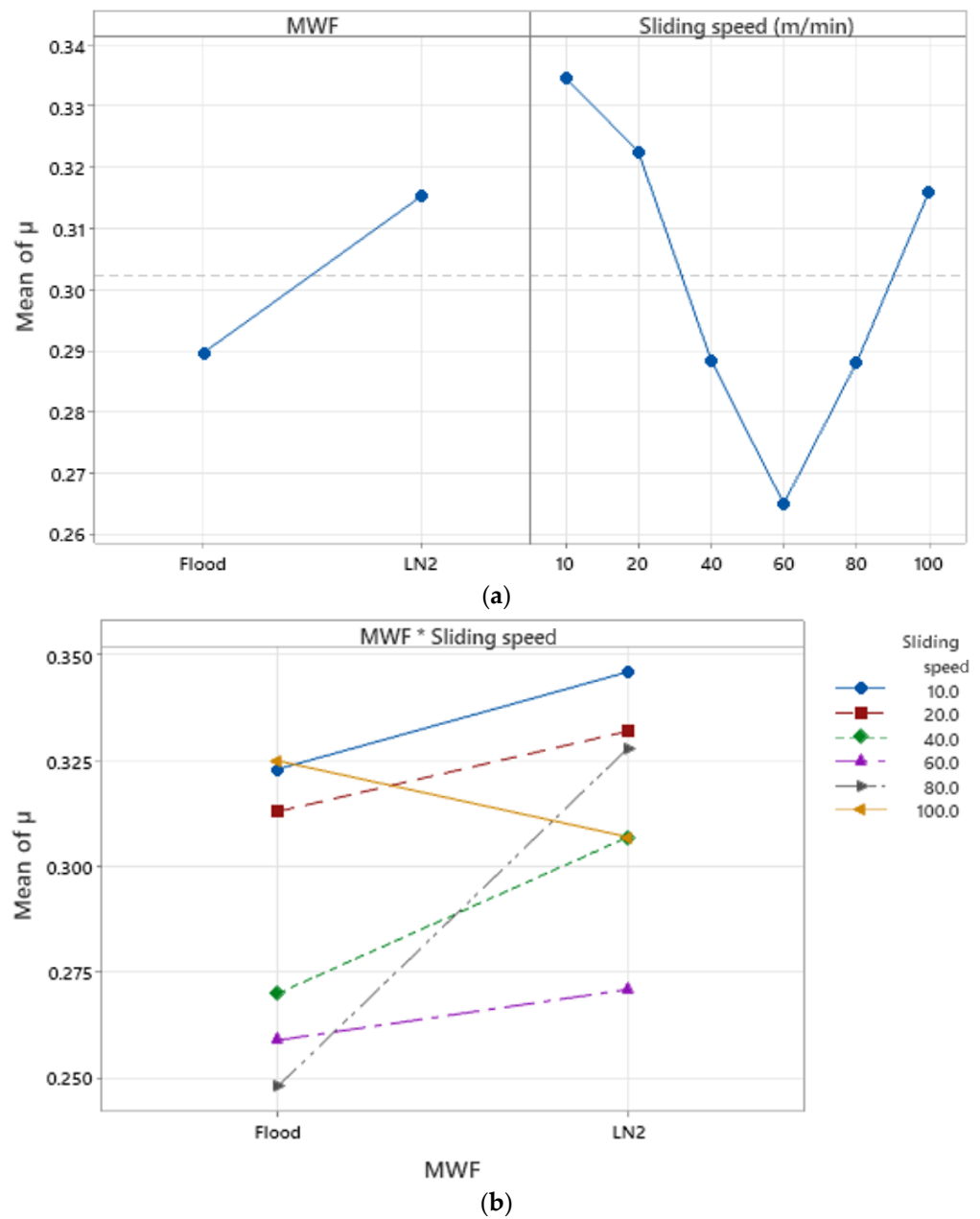


Figure 25. Influence of the (a) type of MWF and sliding speed, and (b) their interactions, on apparent friction coefficient.

To determine the optimal type of MWF and sliding speed to reduce the adhesion of Ti-6Al-4V to pins, and thus the apparent friction coefficient, an optimization analysis was performed. The results are presented in Table 10, and allow us to conclude that flood conditions and a sliding speed of 60 m/min should be used to reduce the adhesion of Ti-6Al-4V to the pins and thus the apparent friction coefficient.

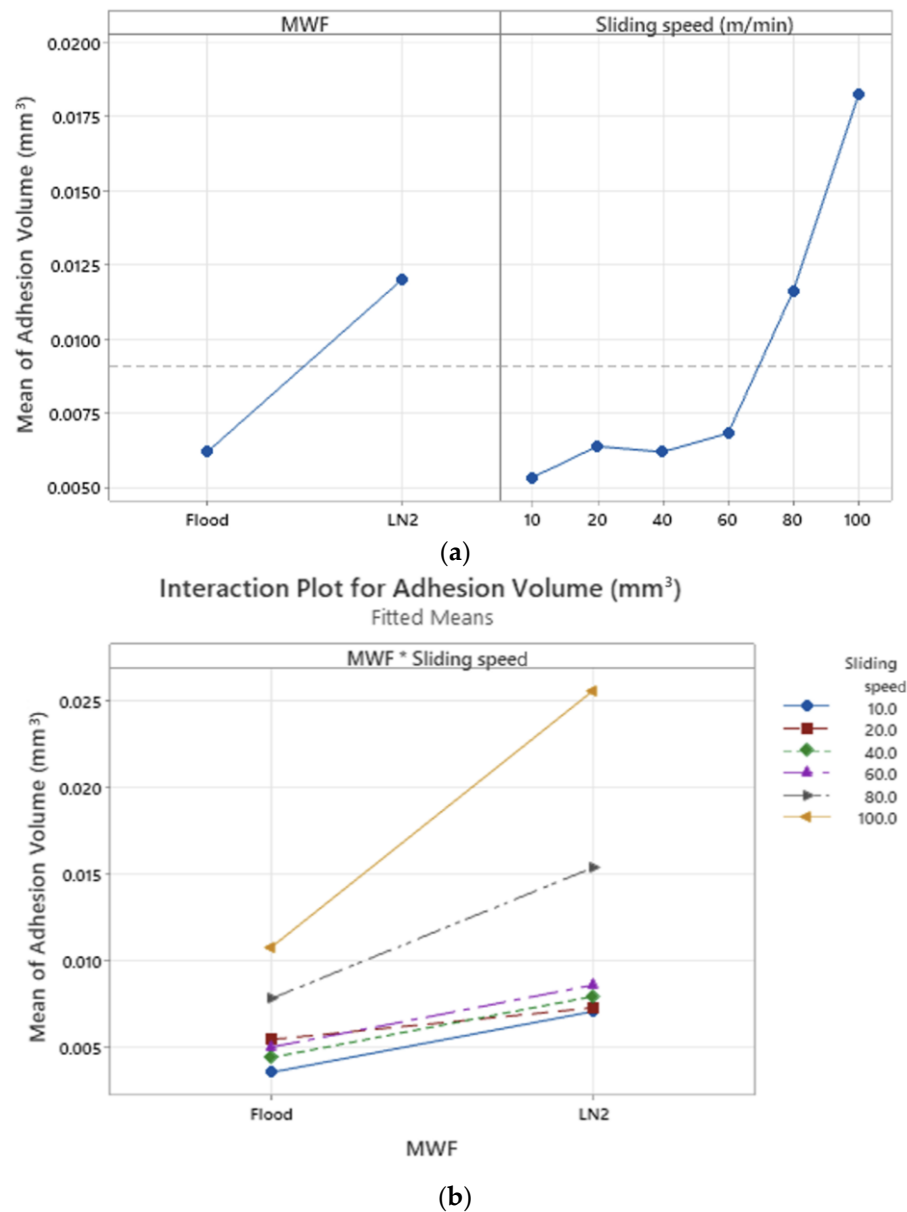


Figure 26. Influence of the (a) type of MWF and the sliding speed, and (b) their interactions, on the volume of the built-up layer of Ti-6Al-4V alloy in the pins.

Table 10. Optimized type of MWF and sliding speed to reduce the adhesion of Ti-6Al-4V to the pins and the apparent friction coefficient.

MWF	Sliding Speed (m/min)	Adhesion Volume (mm ³)	μ	Composite Desirability
Flood	60	0.00507	0.259	0.864

4. Conclusions

The objective of this work was to analyze the tribological conditions and performance of novel coatings specifically developed for cryogenic-assisted machining, in terms of apparent friction coefficient, volume of built-up material (adhesion), and temperature. This analysis was performed on two cooling/lubrication strategies [60]: liquid nitrogen (LN₂) and flood (oil–water mixture). A pin-on-bar tribometer specially designed to reproduce the contact conditions in machining was used to conduct the tribological tests using uncoated and coated pins in contact with a workpiece made of Ti-6Al-4V alloy, with several sliding

speeds and two contact pressures. Four coatings developed in a previous research work [45] were selected for the tribological tests, namely, CrN, AlCrN, M2 and M4.

The results show that, for both cooling/lubrication strategies, the coating has no relevant effect on the apparent friction coefficient. However, the apparent friction coefficient decreased as the sliding speed increased until about 60–80 m/min, and it then increased with the sliding speed until 100 m/min. These values were generally higher under LN₂ when compared to flood conditions. The increase in the apparent friction coefficient after 60–80 m/min was related to the increase in the adhesion of Ti–6Al–4V alloy to the pins under both cooling/lubrication strategies, and this adhesion was higher for LN₂ cooling due to the absence of a lubricant. Increasing the contact pressure from 872 MPa to 1329 MPa decreased the apparent friction coefficient, although the adhesion was higher at 1329 MPa. The temperature measurements in the pins show that the temperature was lower for coated pins compared to uncoated ones. The lowest pin temperature under flood conditions was obtained with the AlCrN coating, while the lowest temperature under LN₂ cooling was obtained in the M4 coating.

The DoE analysis permitted us to identify the sliding speed and cooling/lubrication strategy as the two main factors influencing the friction coefficient and the adhesion of Ti–6Al–4V alloy to the pins, while the type of coating had no relevant effect. The apparent friction coefficient decreased with the increase in the sliding speed until around 60 m/min, then it increased up to 100 m/min. The adhesion volume was almost constant until a sliding speed of 60 m/min, and it then increased up to 100 m/min. LN₂ cooling led to a greater apparent friction coefficient and adhesion volume than the flood conditions, which is attributed to the lack of lubricant used in LN₂. Finally, the optimization analysis permitted us to conclude that flood conditions and a sliding speed of 60 m/min should be used to reduce the adhesion of Ti–6Al–4V to the pins, and consequently reduce the apparent friction coefficient.

Author Contributions: This study is derived from the Ph.D. thesis [45] of the first author Y.Z., and all the experimental tests, results and analyses are from this study. Conceptualization, Y.Z., J.C.O. and C.N.; methodology, Y.Z., J.C.O. and B.M.; software, Y.Z. and J.C.O.; validation, Y.Z., J.C.O. and B.M.; formal analysis, Y.Z., J.C.O. and L.A.D.; investigation, Y.Z. and B.M.; resources, J.C.O. and C.N.; data curation, Y.Z.; writing—original draft preparation, Y.Z. and J.C.O.; writing—review and editing, Y.Z., J.C.O. and C.N.; visualization, Y.Z. and J.C.O.; supervision, J.C.O. and C.N.; project administration, J.C.O. and C.N. All authors have read and agreed to the published version of the manuscript.

Funding: CSC (Number 201708070010-Chinese Scholarship Council) for supporting this research work.

Data Availability Statement: Data available on request due to restrictions of privacy. The data presented in this study are available on request from the corresponding author. The data are not publicly available due to agreement between authors' institutions.

Acknowledgments: The authors would like to thank CSC (Number 201708070010-Chinese Scholarship Council) for supporting this research work. The authors would like to thank EVATEC Tools for providing the pins. The authors want to thank Frédéric Rossi for the support in designing the tribometer, Denis Lagadrillere for the SEM observations and EDS microanalyses, Alex Montagne for the nanoindentation measurement, Andrzej Kusiak for thermal property determination and Gilles Detroyat for his kind technical support.

Conflicts of Interest: The authors declare no conflict of interest.

Abbreviations

The following abbreviations and nomenclature are used in this manuscript:

CCR	Chip compression ratio
R	Resultant force (N)
F _c	Cutting force (N)
F _n	Normal force (N)
F _t	Tangential/trust force (N)

F_x, F_y, F_z	Measured force components (N)
$F_{n,pin}$	Normal force applied to the pin (N)
$F_{n\gamma}$	Normal force (tool/chip interface) (N)
$P_{n\gamma}$	Average contact pressure (tool/chip interface) (MPa)
P_{prob}	Contact pressure at the pin-workpiece interface
V_c	Cutting speed (m/min)
V_1	Chip velocity (m/min)
V_s	Sliding speed (m/min)
h	Uncut chip thickness (mm)
h_1	Chip thickness (mm)
α, α_n	Flank angle ($^\circ$)
γ, γ_n	Rake angle ($^\circ$)
r_n	Cutting edge radius (μm)
b	Width of cut (mm)
μ_{app}	Apparent friction coefficient
μ_{loc}	Local friction coefficient
μ_{plast}	Macroscopic friction coefficient
l_c	Tool-chip contact length (mm)
ϕ	Shear angle (deg.)
A, B, C, m, n	Coefficients of the constitutive model
ϵ_p	Plastic strain
$\dot{\epsilon}$	Plastic strain rate (s^{-1})
R_{pin}	Radius of the pin (mm)
R_{work}	Radius of the workpiece (mm)
R_{eq}	Equivalent radius (mm)
R_a	Arithmetical mean roughness (μm)
R_q	Root mean square roughness (μm)
R_t	Maximum height of the roughness profile (μm)
LN_2	Liquid nitrogen
MQL	Minimum quantity of lubricant

References

- van Luttervelt, C.A.; Childs, T.H.C.; Jawahir, I.S.; Klocke, F.; Venuvinod, P.K.; Altintas, Y.; Armarego, E.; Dornfeld, D.; Grabec, I.; Leopold, J.; et al. Present Situation and Future Trends in Modelling of Machining Operations Progress Report of the CIRP Working Group 'Modelling of Machining Operations'. *CIRP Ann.* **1998**, *47*, 587–626. [[CrossRef](#)]
- Neugebauer, R.; Bouzakis, K.-D.; Denkena, B.; Klocke, F.; Sterzing, A.; Tekkaya, A.E.; Wertheim, R. Velocity effects in metal forming and machining processes. *CIRP Ann.* **2011**, *60*, 627–650. [[CrossRef](#)]
- Rech, J.; Arrazola, P.J.; Claudin, C.; Courbon, C.; Pusavec, F.; Kopac, J. Characterisation of friction and heat partition coefficients at the tool-work material interface in cutting. *CIRP Ann.* **2013**, *62*, 79–82. [[CrossRef](#)]
- Puls, H.; Klocke, F.; Lung, D. A new experimental methodology to analyse the friction behaviour at the tool-chip interface in metal cutting. *Prod. Eng. Res. Dev.* **2012**, *6*, 349–354. [[CrossRef](#)]
- Olsson, M.; Söderberg, S.; Jacobson, S.; Hogmark, S. Simulation of cutting tool wear by a modified pin-on-disc test. *Int. J. Mach. Tools Manuf.* **1989**, *29*, 377–390. [[CrossRef](#)]
- Grzesik, W.; Zalisz, Z.; Nieslony, P. Friction and wear testing of multilayer coatings on carbide substrates for dry machining applications. *Surf. Coat. Technol.* **2002**, *155*, 37–45. [[CrossRef](#)]
- M'Saoubi, R.; Chandrasekaran, H. Innovative Methods for the Investigation of Tool-Chip Adhesion and Layer Formation during Machining. *CIRP Ann.* **2005**, *54*, 59–62. [[CrossRef](#)]
- Kilic, D.S.; Raman, S. Observations of the tool-chip boundary conditions in turning of aluminum alloys. *Wear* **2007**, *262*, 889–904. [[CrossRef](#)]
- Arrazola, P.J.; Ugarte, D.; Domínguez, X. A new approach for the friction identification during machining through the use of finite element modelling. *Int. J. Mach. Tools Manuf.* **2008**, *48*, 173–183. [[CrossRef](#)]
- Grzesik, W.; van Luttervelt, C.A. An Investigation of the Thermal Effects in Orthogonal Cutting Associated with Multilayer Coatings. *CIRP Ann.* **2001**, *50*, 53–56. [[CrossRef](#)]
- Zemzemi, F.; Rech, J.; Salem, W.B.; Dogui, A.; Kapsa, P. Identification of a friction model at tool/chip/workpiece interfaces in dry machining of AISI4142 treated steels. *J. Mater. Process. Technol.* **2009**, *209*, 3978–3990. [[CrossRef](#)]
- Rech, J.; Claudin, C.; D'Eramo, E. Identification of a friction model—Application to the context of dry cutting of an AISI 1045 annealed steel with a TiN-coated carbide tool. *Tribol. Int.* **2009**, *42*, 738–744. [[CrossRef](#)]
- Zemzemi, F.; Bensalem, W.; Rech, J.; Dogui, A.; Kapsa, P. New tribometer designed for the characterisation of the friction properties at the tool/chip/workpiece interfaces in machining. *Tribotest* **2008**, *14*, 11–25. [[CrossRef](#)]

14. Ren, J.; Yuan, H. Contact Analysis and Friction Prediction of Non-Gaussian Random Surfaces. *Appl. Sci.* **2022**, *12*, 11237. [[CrossRef](#)]
15. Goel, S.; Björklund, S.; Curry, N.; Govindarajan, S.; Wiklund, U.; Gaudiuso, C.; Joshi, S. Axial Plasma Spraying of Mixed Suspensions: A Case Study on Processing, Characteristics, and Tribological Behavior of Al₂O₃-YSZ Coatings. *Appl. Sci.* **2020**, *10*, 5140. [[CrossRef](#)]
16. Wu, N.; Hu, N.; Wu, J.; Zhou, G. Tribology Properties of Synthesized Multiscale Lamellar WS₂ and Their Synergistic Effect with Anti-Wear Agent ZDDP. *Appl. Sci.* **2020**, *10*, 115. [[CrossRef](#)]
17. Le, V.N.-A.; Lin, J.-W. Tribological Properties of Aluminum Nanoparticles as Additives in an Aqueous Glycerol Solution. *Appl. Sci.* **2017**, *7*, 80. [[CrossRef](#)]
18. Istrate, B.; Munteanu, C.; Lupescu, S.; Benchea, M.; Vizureanu, P. Preliminary Microstructural and Microscratch Results of Ni-Cr-Fe and Cr₃C₂-NiCr Coatings on Magnesium Substrate. *IOP Conf. Ser. Mater. Sci. Eng.* **2017**, *209*, 012024. [[CrossRef](#)]
19. Smolenicki, D.; Boos, J.; Kuster, F.; Roelofs, H.; Wyen, C.F. In-process measurement of friction coefficient in orthogonal cutting. *CIRP Ann.* **2014**, *63*, 97–100. [[CrossRef](#)]
20. Bonnet, C.; Valiorgue, F.; Rech, J.; Claudin, C.; Hamdi, H.; Bergheau, J.M.; Gilles, P. Identification of a friction model—Application to the context of dry cutting of an AISI 316L austenitic stainless steel with a TiN coated carbide tool. *Int. J. Mach. Tools Manuf.* **2008**, *48*, 1211–1223. [[CrossRef](#)]
21. Meier, L.; Schaal, N.; Wegener, K. In-process Measurement of the Coefficient of Friction on Titanium. *Procedia CIRP* **2017**, *58*, 163–168. [[CrossRef](#)]
22. Wang, Q.; Zheng, F.; Wang, T. Tribological properties of polymers PI, PTFE and PEEK at cryogenic temperature in vacuum. *Cryogenics* **2016**, *75*, 19–25. [[CrossRef](#)]
23. Gradt, T.; Schneider, T.; Hübner, W.; Börner, H. Friction and wear at low temperatures. *Int. J. Hydrogen Energy* **1998**, *23*, 397–403. [[CrossRef](#)]
24. Ostrovskaya, Y.L.; Strel'nitskij, V.E.; Kuleba, V.I.; Gamulya, G.D. Friction and wear behaviour of hard and superhard coatings at cryogenic temperatures. *Tribol. Int.* **2001**, *34*, 255–263. [[CrossRef](#)]
25. Yuhkno, T.P.; Vvedensky, Y.V.; Sentyurikhina, L.N. Low temperature investigations on frictional behaviour and wear resistance of solid lubricant coatings. *Tribol. Int.* **2001**, *34*, 293–298. [[CrossRef](#)]
26. Ostrovskaya, Y.L.; Yuhkno, T.P.; Gamulya, G.D.; Vvedenskij, Y.V.; Kuleba, V.I. Low temperature tribology at the B. Verkin Institute for Low Temperature Physics & Engineering (historical review). *Tribol. Int.* **2001**, *34*, 265–276. [[CrossRef](#)]
27. El-Tayeb, N.S.M.; Yap, T.C.; Venkatesh, V.C.; Brevern, P.V. Modeling of cryogenic frictional behaviour of titanium alloys using Response Surface Methodology approach. *Mater. Des.* **2009**, *30*, 4023–4034. [[CrossRef](#)]
28. Basmaci, G.; Yoruk, A.S.; Koklu, U.; Morkavuk, S. Impact of Cryogenic Condition and Drill Diameter on Drilling Performance of CFRP. *Appl. Sci.* **2017**, *7*, 667. [[CrossRef](#)]
29. Jerold, B.D.; Kumar, M.P. The Influence of Cryogenic Coolants in Machining of Ti–6Al–4V. *J. Manuf. Sci. Eng.* **2013**, *135*, 031005. [[CrossRef](#)]
30. Pahlitzsch, G. Gases are good cutting coolants. *Am. Mach.* **1953**, *97*, 196.
31. Klocke, F.; Krämer, A.; Sangermann, H.; Lung, D. Thermo-Mechanical Tool Load during High Performance Cutting of Hard-to-Cut Materials. *Procedia CIRP* **2012**, *1*, 295–300. [[CrossRef](#)]
32. Bordin, A.; Sartori, S.; Bruschi, S.; Ghiotti, A. Experimental investigation on the feasibility of dry and cryogenic machining as sustainable strategies when turning Ti6Al4V produced by Additive Manufacturing. *J. Clean. Prod.* **2017**, *142*, 4142–4151. [[CrossRef](#)]
33. Bermingham, M.J.; Kirsch, J.; Sun, S.; Palanisamy, S.; Dargusch, M.S. New observations on tool life, cutting forces and chip morphology in cryogenic machining Ti–6Al–4V. *Int. J. Mach. Tools Manuf.* **2011**, *51*, 500–511. [[CrossRef](#)]
34. Bermingham, M.J.; Palanisamy, S.; Dargusch, M.S. Understanding the tool wear mechanism during thermally assisted machining Ti–6Al–4V. *Int. J. Mach. Tools Manuf.* **2012**, *62*, 76–87. [[CrossRef](#)]
35. Sartori, S.; Moro, L.; Ghiotti, A.; Bruschi, S. On the tool wear mechanisms in dry and cryogenic turning Additive Manufactured titanium alloys. *Tribol. Int.* **2017**, *105*, 264–273. [[CrossRef](#)]
36. Strano, M.; Chiappini, E.; Tirelli, S.; Albertelli, P.; Monno, M. Comparison of Ti6Al4V machining forces and tool life for cryogenic versus conventional cooling. *Proc. Inst. Mech. Eng. Part B J. Eng. Manuf.* **2013**, *227*, 1403–1408. [[CrossRef](#)]
37. Sun, S.; Brandt, M.; Palanisamy, S.; Dargusch, M.S. Effect of cryogenic compressed air on the evolution of cutting force and tool wear during machining of Ti–6Al–4V alloy. *J. Mater. Process. Technol.* **2015**, *221*, 243–254. [[CrossRef](#)]
38. Lin, H.; Wang, C.; Yuan, Y.; Chen, Z.; Wang, Q.; Xiong, W. Tool wear in Ti-6Al-4V alloy turning under oils on water cooling comparing with cryogenic air mixed with minimal quantity lubrication. *Int. J. Adv. Manuf. Technol.* **2015**, *81*, 87–101. [[CrossRef](#)]
39. Jawahir, I.S.; Attia, H.; Biermann, D.; Dufflou, J.; Klocke, F.; Meyer, D.; Newman, S.T.; Pusavec, F.; Putz, M.; Rech, J.; et al. Cryogenic manufacturing processes. *CIRP Ann.* **2016**, *65*, 713–736. [[CrossRef](#)]
40. Gupta, K. A Review On Green Machining Techniques, *Procedia Manufacturing*. **2020**, *51*, 1730–1736. [[CrossRef](#)]
41. Pereira, O.; Català, P.; Rodríguez, A.; Ostra, T.; Vivancos, J.; Rivero, A.; López-de-Lacalle, L.N. The Use of Hybrid CO₂+MQL in Machining Operations. *Procedia Eng.* **2015**, *132*, 492–499. [[CrossRef](#)]
42. Rech, J.; Kusiak, A.; Battaglia, J.L. Tribological and thermal functions of cutting tool coatings. *Surf. Coat. Technol.* **2004**, *186*, 364–371. [[CrossRef](#)]
43. Sadik, M.I.; Isakson, S. The role of PVD coating and coolant nature in wear development and tool performance in cryogenic and wet milling of Ti–6Al–4V. *Wear* **2017**, *386–387*, 204–210. [[CrossRef](#)]

44. Lequien, P. Fundamental Study of Cryogenic Assistance for Milling Application of Ti6Al4V. Ph.D. Thesis, Ecole Nationale Supérieure d'Arts et Métiers—ENSAM, Paris, France, 2017. Available online: <https://pastel.archives-ouvertes.fr/tel-01743850> (accessed on 13 September 2018).
45. Zhang, Y. Tool Materials Development for Improved Performance of Cutting Tools in Cryogenic Machining of Aeronautic Alloys. Ph.D. Thesis, Ecole Nationale Supérieure d'Arts et Métiers—ENSAM, Paris, France, 2022. Available online: <https://www.theses.fr/2022HESAE009> (accessed on 9 July 2022).
46. Challen, J.M.; Oxley, P.L.B. An explanation of the different regimes of friction and wear using asperity deformation models. *Wear* **1979**, *53*, 229–243. [[CrossRef](#)]
47. Zvorykin, K.A. On the force and energy necessary to separate the chip from the workpiece. *Vetnik Promyslennostie*. **1896**, 123.
48. Cheng, W.; Outeiro, J.C. Modelling orthogonal cutting of Ti–6Al–4V titanium alloy using a constitutive model considering the state of stress. *Int. J. Adv. Manuf. Technol.* **2022**, *119*, 4329–4347. [[CrossRef](#)]
49. Astakhov, V.P. *Tribology of Metal Cutting*; Tribology and Intergace Engineering Series, 52; Briscoe, B.J., Ed.; Elsevier: Amsterdam, The Netherlands, 2006.
50. Outeiro, J.C.; Umbrello, D.; M'Saoubi, R.; Jawahir, I.S. Evaluation of Present Numerical Models for Predicting Metal Cutting Performance and Residual Stresses. *Mach. Sci. Technol.* **2015**, *19*, 183–216. [[CrossRef](#)]
51. Melkote, S.N.; Grzesik, W.; Outeiro, J.; Rech, J.; Schulze, V.; Attia, H.; Arrazola, P.-J.; M'Saoubi, R.; Saldana, C. Advances in material and friction data for modelling of metal machining. *CIRP Ann.* **2017**, *66*, 731–754. [[CrossRef](#)]
52. Cheng, W.; Outeiro, J.; Costes, J.-P.; M'Saoubi, R.; Karaouni, H.; Astakhov, V. A constitutive model for Ti6Al4V considering the state of stress and strain rate effects. *Mech. Mater.* **2019**, *137*, 103103. [[CrossRef](#)]
53. Combres, Y. Propriétés du titane et de ses alliages. *Tech. Ing. Matér. Mét.* **1999**, MB5, M557.1–M557.15. [[CrossRef](#)]
54. Upadhyaya, G.S. Materials science of cemented carbides—An overview. *Mater. Des.* **2001**, *22*, 483–489. [[CrossRef](#)]
55. Ruoff, A.L.; Wanagel, J. Yield stress of cemented tungsten carbide. *J. Appl. Phys.* **1975**, *46*, 4647–4648. [[CrossRef](#)]
56. Johnson, G.R.; Cook, W.H. Fracture characteristics of three metals subjected to various strains, strain rates, temperatures and pressures. *Eng. Fract. Mech.* **1985**, *21*, 31–48. [[CrossRef](#)]
57. Courbon, C.; Pusavec, F.; Dumont, F.; Rech, J.; Kopac, J. Tribological behaviour of Ti6Al4V and Inconel718 under dry and cryogenic conditions—Application to the context of machining with carbide tools. *Tribol. Int.* **2013**, *66*, 72–82. [[CrossRef](#)]
58. Hertz, H. On the contact of elastic solids. *Z. Reine Angew. Math.* **1881**, *92*, 156–171.
59. Hills, D.A.; Nowell, D.; Sackfield, A. *Mechanics of Elastic Contacts*, 1993; Butterworth-Heinemann: London, UK, 1998; Volume 21, pp. 235–237.
60. Astakhov, V.P.; Joksch, S. *Metalworking Fluids (MWFs) for Cutting and Grinding: Fundamentals and Recent Advances*, 1st ed.; Woodhead Publishing: Cambridge, UK; Philadelphia, PA, USA; New Delhi, India, 2012.

Disclaimer/Publisher's Note: The statements, opinions and data contained in all publications are solely those of the individual author(s) and contributor(s) and not of MDPI and/or the editor(s). MDPI and/or the editor(s) disclaim responsibility for any injury to people or property resulting from any ideas, methods, instructions or products referred to in the content.